Published OnlineFirst January 7, 2020; DOI: 10.1158/0008-5472.CAN-19-2374

The Immunosuppressive Microenvironment in BRCA1-IRIS–Overexpressing TNBC Tumors Is Induced by Bidirectional Interaction with Tumor-Associated Macrophages

Eman Sami[1], Bibbin T. Paul[2], James A. Koziol[3], and Wael M. ElShamy[1]

ABSTRACT

Tumor-associated macrophages (TAM) promote triple-negative breast cancer (TNBC) progression. Here, we report BRCA1-IRIS–overexpressing (IRISOE) TNBC cells secrete high levels of GM-CSF in a hypoxia-inducible factor-1α (HIF1α)- and a NF-κB–dependent manner to recruit macrophages to IRISOE cells and polarize them to protumor M2 TAMs. GM-CSF triggered TGFβ1 expression by M2 TAMs by activating STAT5, NF-κB, and/or ERK signaling. Despite expressing high levels of TGFβ1 receptors on their surface, IRISOE TNBC cells channeled TGFβ1/TβRI/II signaling toward AKT, not SMAD, which activated stemness/EMT phenotypes. In orthotopic and syngeneic mouse models, silencing or inactivating IRIS in TNBC cells lowered the levels of circulating GM-CSF, suppressed TAM recruitment, and decreased the levels of circulating TGFβ1. Coinjecting macrophages with IRISOE TNBC cells induced earlier metastasis in athymic mice accompanied by high levels of circulating GM-CSF and TGFβ1. IRISOE TNBC cells expressed low levels of calreticulin (the "eat me" signal for macrophages) and high levels of CD47 (the "do not eat me" signal for macrophages) and PD-L1 (a T-cell inactivator) on their surface. Accordingly, IRISOE TNBC tumors had significantly few $CD8^+/PD\text{-}1^+$ cytotoxic T cells and more $CD25^+/FOXP3^+$ regulatory T cells. These data show that the bidirectional interaction between IRISOE cells and macrophages triggers an immunosuppressive microenvironment within TNBC tumors that is favorable for the generation of immune-evading/stem-like/IRISOE TNBC metastatic precursors. Inhibiting this interaction may inhibit disease progression and enhance patients' overall survival.

Significance: The BRCA1-IRIS oncogene promotes breast cancer aggressiveness by recruiting macrophages and promoting their M2 polarization.

Introduction

Evading immune system destruction is an effective strategy for cancer progression. This tolerogenic environment induced by factors released from tumor cells expands protumor myeloid cells, such as macrophages (1). Tumor-associated macrophages (TAM) can be polarized to antitumor, M1 macrophages that express metabolic enzymes, such as iNOS, cytokines, such as IL12, chemokines, such as CXCL10, and transcription factors, such as IRF5 (2), or protumor, M2 macrophages that express metabolic enzymes, such as ARG1, cytokines, such as IL10, chemokines, such as CCL17, and transcription factors, such as IRF4 (1, 2).

GM-CSF stimulates proliferation and survival of macrophages, neutrophils, eosinophils, dendritic cells (DC), and microglia (3). GM-CSF also affects mature hemopoietic cells through cytokines production, antigen presentation, and phagocytosis (4, 5). In mice and human, increased circulated GM-CSF level indicates late-stage tumors and/or tumor progression (6). At low level, GM-CSF exerts an antitumor effect by activating DC within the tumor, while at high level, GM-CSF activity is mainly immunosuppressive, enriching tumor microenvironment of M2 TAMs (7).

Increased expression of the CD47 on cancer cell transduces a "do not eat me" inhibitory signal through activating signal regulatory protein alpha (SIRPα) on macrophages (8). Preclinical models showed anti-CD47 therapies stimulate phagocytosis of cancer cells, *in vitro*, and antitumor immune responses, *in vivo* (8). In contrast, calreticulin expression at the cancer cell surface promotes phagocytosis of cancer cells by engaging the LRP1 receptor on macrophages (9).

The immunoinhibitory receptor, PD-1, is predominantly expressed on activated effector T cells (10), or antigen-specific T cells chronically exposed to the antigen (11). PD-1 ligands, PD-L1 are expressed on hematopoietic and cancer cells, and PD-L2 is expressed on macrophages and DCs (12). PD-L1 on aggressive tumor cells engagement of PD-1 on T cells leads to T-cell exhaustion (i.e., anergy) including inhibition of proliferation and cytokines, for example, IL2 and IFNγ production, and apoptosis, resulting in tumor cells evasion of recognition/destruction by the immune system (13, 14). Anti-PD-1 or anti-PD-L1 is now a successful cancer immunotherapy that stimulates the adaptive immune system to attack cancer cells (14).

BRCA1-IRIS (i.e., IRIS, in-frame reading of intron 11 splice variant) is an oncogene produced by the alternative usage of the *BRCA1* locus (15). IRIS expression is high in breast cancers, especially triple-negative breast cancers (TNBC; ref. 16). Deliberate IRIS overexpression (IRISOE) in normal human mammary epithelial (HME) cells or luminal A/ER^+ cells converts them into genuine TNBC cells expressing basal, epithelial-to-mesenchymal (EMT), and stemness

[1]Breast Cancer Program, San Diego Biomedical Research Institute, San Diego, California. [2]Department of Molecular Biology and Biophysics, University of Connecticut Health Center, Farmington, Connecticut. [3]Department of Molecular and Experimental Medicine, The Scripps Research Institute, La Jolla, California.

Note: Supplementary data for this article are available at Cancer Research Online (http://cancerres.aacrjournals.org/).

Corresponding Author: Wael M. ElShamy, San Diego Biomedical Research Institute, 10865 Road to Cure, San Diego, CA 92121. Phone: 858-200-7195; Fax: 858-200-7096; E-mail: welshamy@sdbri.org

Cancer Res 2020;80:1102–17

doi: 10.1158/0008-5472.CAN-19-2374

Published OnlineFirst January 7, 2020; DOI: 10.1158/0008-5472.CAN-19-2374

markers, and lacking ERα and BRCA1 proteins expression, *in vitro* and *in vivo* (17). HME/IRISOE cells formed genuine TNBCs in SCID mice (16, 18), including the presence of a necrotic/hypoxic/inflamed cores within them (16, 19). We recently named this core "the aggressiveness niche" (19), and showed experimental evidence that IRISOE TNBC metastatic precursors develop within this aggressiveness niche (18, 20, 21).

Here, we show that GM-CSF secretion from IRISOE cells activates STAT5, NF-κB, and ERK signaling in TAMs to enhance their proliferation, recruitment, survival, M2 polarization, and expression/secretion of TGFβ1. Inhibiting GM-CSF signaling attenuated TAMs recruitment and M2 polarization and decreased the immunosuppressive ability of IRISOE cells, leading to significantly reduced aggressiveness and regression of IRISOE tumors through an activated adaptive immune response.

Materials and Methods

Cell culture

Mammary cell lines used here were from the ATCC and maintained as described previously (18). The doxycycline-inducible IRISOE cell lines (IRISOE1–5) generation and maintenance were described earlier (15). Orthotopic injection of these cell lines in SCID mice and maintaining mice on doxycycline-supplemented drinking water led to primary (1°) orthotopic IRISOE mammary tumors. Few of these tumors used to develop 1° orthotopic IRISOE breast cancer cell lines "IRIS291, IRIS292, and IRIS293" were used in the experiments described herein (16, 18). These cell lines were maintained in doxycycline-supplemented RPMI1640 medium containing 10% FBS. IRIS291 and IRIS293 clones expressing red fluorescent protein (RFP) were developed by a viral infection of a mCherry-expressing cDNA and antibiotic selection. Human THP1s from ATCC were maintained in PRMI/10% FBS in our laboratory. Authentication of all commercial and in-house cell lines was done using short tandem repeat profiling and also tested for *Mycoplasma* contamination.

Antibodies, recombinant proteins, and drugs

Mouse monoclonal (mono) anti-human IRIS and rabbit polyclonal (poly) anti-mouse Iris antibodies were developed in our laboratory. Mouse anti-human GM-CSF (R&D Systems, catalog no. 3209), Rabbit (Rb) poly-anti-mouse GM-CSF (ab9741), mouse mono-anti-human HIF1α (Novus Biological, NB100–105), Rb poly-anti-human p-p65/NF-κB (Cell Signaling Technology, catalog no. 3033), Rb poly-anti-human γ-tubulin (Abcam, ab11321), Rb mono-anti-human Actin (Cell Signaling Technology, 13E5), Rat mono-anti-human GM-CSF Rα (R&D Systems, catalog no. 698423), mouse mono-anti-human and -mouse TGF-β1 (R&D Systems, catalog no. 9016), Rb poly-anti-human TβRII (Y^{424}, sc-17007-R), Rb poly-anti-human cyclin D1 (Thermo Fisher Scientific, catalog no. RB-010-P0), Rb poly-anti-human p-SMAD2 (S^{465}, S^{467}, Thermo Fisher Scientific, 44–244G), Rb mono-anti-human p-SMAD3 (S^{423}, S^{425}, Cell Signaling Technology, C25A9), mouse mono-anti-mouse and -human TGFβ1 (Bio-Cell, 704719J1), FITC-conjugated rat mono-anti-human- and mouse-CD11b and isotype control (Cell Signaling Technology, catalog nos. 24442 and 56722, respectively), F4/80 Rat mono-anti-mouse F4/80 (Abcam, ab6640), PE-conjugated mono-mouse anti-human CD206 and isotype control (Invitrogen, 12–2069, P3.6.2.8.1, respectively), Rat mono-anti-mouse CD25 (Abcam, ab210333), Rb mono-anti-human and -mouse FOXP3 (Abcam, ab215206), Rat mono-anti-mouse CD8 (BioLegend, 100702), Rb poly- anti-human Calreticulin (R&D Systems, catalog no. 681233), Rb mono-anti-human PD-L1 (Abcam, ab251611).

Human recombinant GM-CSF was obtained from R&D Systems (7954-GM), reconstituted in sterile PBS to a stock concentration of 100 μg/mL, and used at 50 ng/mL. Human recombinant EGF was obtained from Cell Signaling Technology (catalog no. 8916), reconstituted in sterile PBS to a stock solution of 100 μg/mL, and used at 10 ng/mL. Human recombinant TGFβ1 was obtained from R&D Systems (7754-BH), reconstituted in 4 mmol/L HCl to a stock concentration of 100 μg/mL, and used at 5 ng/mL. Vehicles for these recombinant proteins were PBS and/or 0.2 μmol/L HCl.

The NF-κB inhibitor JSH-23 from Sigma (catalog no. J4455, 10 μmol/L working concentration), the STAT5 inhibitor IQDMA from Abcam (ab141192, 10 μmol/L working concentration), the NF-κB inhibitor Bay 11–7082 from Sigma (B5556; 10 μmol/L working concentration), the ERK inhibitor PD98059 from Calbiochem (catalog no. 51300; 10 μmol/L working concentration), the PI3K inhibitor LY294002 from Calbiochem (catalog no. 440202; 10 μmol/L working concentration), the SMAD3 inhibitor SIS3 from Calbiochem (catalog no. 566405; 10 μmol/L working concentration), and the TβRI/II inhibitor LY2109761 from Santa Cruz Biotechnology (700874-71-1; 5 μmol/L working concentration).

Cytokine array

Conditioned media (CM) from equal numbers from IRISOE cell lines (IRIS1–IRIS5) grown in the absence (i.e., naïve HME) or the presence (i.e., HME/IRIS) of doxycycline plated in serum-free medium for 20 hours used to screen for cytokine, chemokine, and growth factors levels on antibody arrays (RayBio). Assay performed according to the manufacturer's instructions and as described previously (22) repeated on three different preparations (i.e., $n = 3$ for each cell line in the presence or absence of doxycycline).

siRNA transfection

Naïve HME, IRIS291, and IRIS293 cells seeded at a density of 3×10^5 cells/well in a 6-well plate for 16–18 hours transiently transfected with siLuc siRNA, siHIF1α (using two different siRNA), siGM-CSF, siTGF-β1, siSMAD5, sip65, siERK, or siIRIS using Xfect Transfection Reagent (Clontech) according to the manufacturer's instructions. After 48 hours, media was changed, and cells exposed to normoxia (20% O_2) or hypoxia [1% O_2, using hypoxia chamber (STEMCELL Technologies, catalog no. 27310)] for an additional 24 hours, at which time, CM collected for ELISA analysis and total proteins for Western blot. At least $n = 3$ for each assay was performed.

CM transfer experiment

Briefly, CM from normoxic or hypoxic (24 hours) naïve HME, IRIS291, IRIS292, or IRIS293 directly analyzed for secreted factors using ELISA or receptors expression using membrane preparations. The CM following certain siRNA transfection or hypoxia was added onto THP1 cells. Secretion from THP1 was assessed using ELISA 24 hours later, and receptor expression on the surface was determined using Western blot analysis of membrane extracts. At all steps, equal numbers of each cell type were seeded to avoid discrepancies due to cell number variations. At various steps in this protocol, specific NeuAb and/or drugs were added, as indicated in the Results section.

Cytokine ELISA

Cocultures CM or mice sera diluted in carbonate coating buffer (pH 9.6) was used to coat 96-well ELISA plates overnight at 4°C. Plates were then washed three times with phosphate-buffered saline - 0.05% Tween-20 (PBS-T) and blocked with 2% BSA for 1 hour at room

Published OnlineFirst January 7, 2020; DOI: 10.1158/0008-5472.CAN-19-2374

temperature were incubated with primary antibody diluted in blocking solution for 2 hours at room temperature. After washing primary antibodies, horseradish peroxidase (HRP)-conjugated secondary antibodies were added for 1 hour at room temperature, and the reaction was determined using Western Lightning Plus-ECL (PerkinElmer) as a substrate. All experiments were done in triplicates, performed three separate times, and shown as mean ± SD.

Coculture experiment

Boyden chambers (BD Biosciences) of 8-μm pore size (for migration) or 0.4-μm pore size (for secretome) analysis were used to layer IRISOE cells in the bottom chamber with or without neutralizing antibodies and the THP1 cells in the transwell inserts. THP1s migrated to the lower face of these inserts and were counted and plotted 24–72 hours later. Cocultures were performed under normoxic or hypoxic conditions, in triplicates three separate times.

Western blot analysis

Western blot analysis was performed as described previously (22). Protein lysates were prepared from cell sonication (in PBS containing protease and phosphatase inhibitor, Thermo Fisher Scientific) or membrane fraction. Protein concentrations were estimated using Pierce BCA Protein Assay Kit (Thermo Fisher Scientific) and 25 μg of proteins was denatured in NuPAGE LDS Sample Buffer (Thermo Fisher Scientific) were resolved on NuPAGE Gels (Thermo Fisher Scientific). Proteins were electro-transferred to polyvinylidene difluoride membranes that were blocked with 5% dry milk for 1 hour, washed five times (10 minutes/each) with PBS-T. Incubation with primary antibody was always done overnight at 4°C when membranes were again washed five times (10 min/each) with PBS-T and exposed to suitable HRP-conjugated secondary antibodies for 1 hour at room temperature. Washed membranes were developed using Western Lightning Plus-ECL as a substrate. Tubulin or actin was used as an internal loading control. All Western blots were done at least three separate times.

IHC

IHC analysis as described previously (22), was done on 4-μm thick paraffin-embedded sections of tumor tissue excised from IrisOE syngeneic mammary tumors generated in BALB/c mice. After deparaffinization and rehydration, antigen retrieval for Iris was performed using pepsin (10 μmol/L) for 20 minutes at 37°C, whereas for all other antigens by boiling the slides in citrate buffer (pH 6.0) for 10 minutes in a microwave. Cooled slides were washed in PBS (3 × 15 minutes each), incubated in 3% hydrogen peroxide (H_2O_2) for 10 minutes to block endogenous peroxidase activity unless fluorescence analyses were performed. Following washing, slides were blocked with 10% normal goat serum for 1 hour at room temperature and probed with primary antibodies overnight at 4°C in a moist chamber. Slides were then incubated with suitable HRP, or Alexa Fluor–conjugated secondary antibodies for 1 hour at room temperature (depending on the analysis). After washing, HRP-conjugated secondary antibody–treated slides were developed using Vector DAB Substrate Kit (Vector Laboratories) and counterstained with Meyer hematoxylin (Thermo Fisher Scientific) for 2 minutes, washed, dehydrated, and mounted with Permount (Thermo Fisher Scientific). Alternatively, slides that were stained with Alexa Fluor–conjugated secondary antibody were counterstained and mounted with VECTASHIELD mounting medium for fluorescence with DAPI (Vector Laboratories) and were imaged under the microscope. All experiments were done on at least five tumors from phenotypes or treatments.

RT-PCR and real-time qRT-PCR

One-hundred nanogram of total RNA was processed for qRT-PCR using iScript One-Step RT-PCR Kit with SYBR Green (Bio-Rad) using *EGFR mRNA*, forward: 5′-CCAGGACCCCCACAGCACTGCAGTGGGCAA-3′, reverse: 5′-GTGGGTCTAAGAGCTAATGCGGGCATGGCT-3′; *CK5 mRNA*, forward: 5′-GCGGTTCCTGGAGCAGCAGAACAAGGTTCT-3′, reverse: 5′-CTGAGGTGTCAGAGACATGCGTCTGCATCT-3′; *CK17 mRNA*, forward: 5′-CTGGCTGCTGATGACTTCCGCACCAAGTTT-3′, reverse: 5′-CGCAGTAGCGGTTCTCTGTCTCCGCCAGGT-3′; *CDH2 mRNA*, forward: 5′-ACAGTGGCCACCTACAAAGG-3′, reverse: 5′-CCGAGATGGGGTTGATAATG-3′; *Twist mRNA*: forward: 5′-GGAGTCCGCAGTCTTACGAG-3′, reverse: 5′-TCTGGAGGACCTGGTAGAGG-3′; *SnailI mRNA*, forward: 5′-CCTCCCTGTCAGATGAGGAC-3′, reverse: 5′-CCAGGCTGAGGTATTCCTTG-3′; *Sox2 mRNA*, forward: 5′-TTCATCGACGAGGCTAAGCGGCTG-3′, reverse: 5′-AGCTGCCGTTGCTCCAGCCGTTCA-3′; *Oct4 mRNA*, forward: 5′-ACATGTGTAAGCTGCGGCC-3′, reverse: 5′-GTTGTGCATAGTCGCTGCTTG-3′; and *Nanog mRNA*, forward: 5′-ATGCCTCACACGGAGACTGT-3′, reverse: 5′-AGGGCTGTCCTGAATAAGCA-3′. The following primers for *β-actin mRNA* (internal control), forward: 5′-ACAGAGCCTCGCCTTTGC-3′, reverse: 5′-GCGGCGATATCATCATCC-3′ were used to normalize with expression and data were correlated to the calibrator sample.

The qPCR reactions were performed in a final volume of 25 μL. The mean C_t was calculated for each sample and used to determine the ΔC_t for this sample as follows: $\Delta C_T = C_t$ for the gene of interest − C_t of the internal control gene (β-actin). Then the $\Delta\Delta C_T$ was calculated as follows: $\Delta\Delta C_T = [(C_t$ for the gene of interest − C_t of the internal control gene, β-actin) for sample A − (C_t for the gene of interest − C_t of the internal control gene (β-actin) for sample B], where sample B is the calibrator. For the statistical analysis, the $\Delta\Delta C_T$ and not the raw C_t data were used (23). All were done in triplicates, performed three separate times.

FACS

Single-cell suspensions from the *in vivo*–treated tumors were processed for FACS analysis. One million cells were stained with specific fluorescently labeled antibodies on ice for 1 hour. Cells were then washed three times with FACS buffer (1% BSA in PBS) by centrifugation at 2,000 rpm at 4°C for 10 minutes, and further incubated with FITC-conjugated secondary antibody for 30 minutes in ice. Cells were washed and then analyzed for surface staining on Gallios Flow Cytometer (Beckman Coulter). For sorting, Moflo XDP Cell Sorter (Beckman Coulter) was used. The data were analyzed with Kaluza Flow Cytometry Analysis Software v 1.2. Each FACS was performed three separate times in triplicates with identical results.

Orthotopic and syngeneic mammary models

All animal experiments were approved by the Institutional Animal Care and Use Committee of the University of Mississippi Medical Center and in accordance with the NIH guidelines. Athymic or BALB/c (6–8 weeks old) female mice (numbers are indicated in Results) were injected in the second left thoracic mammary fat pad with orthotopic 1° IRISOE mammary tumor cell lines: IRIS291 or IRIS293 (also RFP-expressing variants), or the human IRISOE/TNBC cell lines, MDA-MB-231 (hereafter, MDA231) or MDA-MB-468 (hereafter, MDA468) cell lines (17, 19–21) expressing shCtrl or shIRIS, or the mouse TNBC cell line, 4T1 expressing shCtrl or shIris1 or shIris2, admixed or not with human THP1-macrophages (at 10:1

Published OnlineFirst January 7, 2020; DOI: 10.1158/0008-5472.CAN-19-2374

ratio). After IRISOE tumors reached a tumor volume indicated in figures and text, randomized mice were divided into groups that were injected intratumorally with vehicle or IRISpep four times every third day for 2 weeks. Tumor formation or death was monitored and recorded, as indicated in text and figures. A digital caliper was used to measure tumors every third day, and volume was calculated using the formula: volume = (length × width^2)/2. Endpoints were death or sacrifice of mice and a collection of tumors and peripheral blood. Excised tumors were divided into several portions, flash-frozen to generate DNAs, RNAs, and proteins, and prepare single cells as described in (24) for FACS analysis as indicated, or paraffin embedding, sectioning (at 4 μm), and IHC staining as described above.

Human samples staining and analysis

Kaplan–Meier plotter was used to delineate the association between IRIS gene expression and disease-free survival (DFS) or overall survival (OS). Within each cohort, high expresser and low expresser patients were analyzed and compared for their OS and DFS, respectively. Breast tissue microarrays comprised of normal, DCIS, and invasive and metastatic samples were purchased from US Biomax, Inc. IHC protocols were described earlier (16). A semiquantitative scoring system was used to identify the percentage of tumor cells showing positive staining (25). Scoring represents the overall stain intensity and percentage of cancer cells stained in four high-magnification fields of each sample. Average overall staining intensity (26) was valued as percentage of cell stained/field: zero (<1% staining) was considered very weakly stained, 1 (1%–10% staining) was considered weakly stained, 2 (10%–25% staining) was considered medium stained, 3 (25%–50% staining) was considered strongly stained, and 4 (>50% staining) was considered very strongly stained. The positive staining scoring method is subjective, and artifacts such as high background or variable stain deposition can skew the results, and the scores for the two categories remain as separate functions and cannot be combined for analysis and comparison (27).

The study also involves a cohort of 96 patients with breast cancer with primary invasive ductal carcinomas recently diagnosed and treated at the NCI (Bethesda, MD) and Cairo University, (Cairo, Egypt) between September 2009 and October 2012, were included in the study as recently reported by us (28). None of the patients showed metastasis at the time of the initial diagnosis. Expression of estrogen receptor, progesterone receptor, and HER2/neu was assessed in all tumor samples. On the basis of this analysis 43 of the patients were negative for all three markers and thus considered TNBCs (mean age of 51.91 ± 12.34 SD, range: 30–78 years) and 53 showed expression of some/all of the markers and thus were considered non-TNBCs (mean age of 52.77 ± 12.13 SD, range: 27–81 years). Twenty normal breast tissue samples obtained from reduction mammoplasty (mean age 35 ± 13.94 SD; range, 22–64 years) were included as controls in the study. World Health Organization classification of breast tumors was used to grade the tumors, and American Joint Committee on Cancer's Staging Manual (7th edition) was used to stage the tumors (29). All participants signed written informed consent before enrollment in the study that was approved by the Institutional Review Board of the NCI (Cairo, Egypt), according to the 2011 Helsinki Declaration, CIOMS, Belmont Report, and U.S. Common Rule. Patients enrolled in the study were ≥18 years old, and none of the patients were pregnant or breast feeding, and had an active second malignancy; were involved in another clinical trial were excluded from the study. The median follow-up period was 33 months.

Statistical analysis

Statistical analysis was performed using unpaired, two-tailed Student *t* test. In all figures, data represents the mean from at least three separate biological repeats done in at least triplicates each ± SD; *, $P < 0.05$; **, $P < 0.01$; and ***, $P < 0.001$.

Results

IRIS expression in breast cancers

IHC analysis of paraffin-embedded breast cancer TMAs ($n = 511$, Biomax.us) with a monoclonal anti-IRIS antibody (16) showed low expression in normal/near cancer tissues ($n = 66$, Supplementary Fig. S1A$_1$), increased in the DCIS tumors ($n = 180$, Supplementary Fig. S1A$_2$), increased further in invasive tumors ($n = 100$, Supplementary Fig. S1A$_3$) to reach the highest level in metastatic tumors ($n = 165$, Supplementary Fig. S1A$_4$).

IHC staining of another TMA ($n = 326$, all subtypes, Hawaiian SEER collection) with anti-IRIS, -AKT1, -AKT2, or -p-AKT specific antibodies (16) showed 84% (274/326) of the tumors were IRISOE (i.e., express ≥2-fold over normal tissues). Among those, 64% (176/274, $P = 0.012$), 65% (180/274, $P = 0.006$), 68% (188/274, $P = 0.030$) stained positive for AKT1, AKT2, and p-AKT, respectively (Supplementary Fig. S1B, left; ref. 16). In a TNBC sub-cohort ($n = 72$), 88% (63/72) were IRISOE tumors (16). Spearman correlation coefficient (r) analysis showed $r = 0.748$ ($P = 0.00043$) for IRIS and AKT1 or AKT2 overexpression, and $r = 0.834$ ($P = 0.0038$) for IRIS and p-AKT overexpression (Supplementary Fig. S1B, right).

We reassessed an Egyptian breast cancer cohort ($n = 96$) that contained 45% patients with TNBC and 55% patients with non-TNBC (28). Among the TNBC group, 65% (28/43), while 28% (15/53) among the non-TNBCs group were IRISOE patients (28). Only in the TNBC group, DFS ($P = 0.05$) and OS ($P = 0.04$) were significantly different between IRISOE and IRIS^{low} patients (compare right with left, Supplementary Fig. S1C). Together, these data suggest that in TNBCs, the increase in IRIS and AKT1/2 expression/activation correlates with enhanced breast cancer aggressiveness, and reduced DFS and OS.

GM-CSF recruits TAMs to IRISOE cells

Reanalysis of our recent antibody array screening for IRISOE cells secretome showed that compared with HME cells, CM of IRISOE cells contained >18-fold higher GM-CSF (CSF2, **Fig. 1A**), while same levels CSF3 (**Fig. 1A**). Recently, we proposed that the necrotic/hypoxic/inflamed core within an IRISOE TNBC tumor represents an "aggressiveness niche" (19), where IRISOE TNBC metastatic precursors are developed through bidirectional interactions between IRISOE TNBC cells and activated stromal cells, for example, MSCs and TAMs (20, 21).

To evaluate the aggressiveness niche microenvironment role in GM-CSF production and secretion, siLuc- or siHIF1α–transfected HME, IRIS291, and IRIS293 cells (48 hours) were exposed to normoxia (20% O_2) or hypoxia (1% O_2, for 24 hours). First, as we recently reported even under normoxic conditions, IRISOE cells maintain high levels of HIF1α (**Fig. 1B**). Second, ELISA analysis showed that normoxic siLuc-transfected HME cells secrete low levels of GM-CSF (**Fig. 1C**). Hypoxia and HIF1α silencing did not alter that (**Fig. 1C**). In contrast, normoxic siLuc-transfected IRIS291 or IRIS293 cells secreted approximately 5-fold higher GM-CSF that increased under hypoxia to 15- to 20-fold (**Fig. 1C**). HIF1α silencing (**Fig. 1B**) in IRISOE cells decreased GM-CSF secretion in normoxic and hypoxic

Published OnlineFirst January 7, 2020; DOI: 10.1158/0008-5472.CAN-19-2374

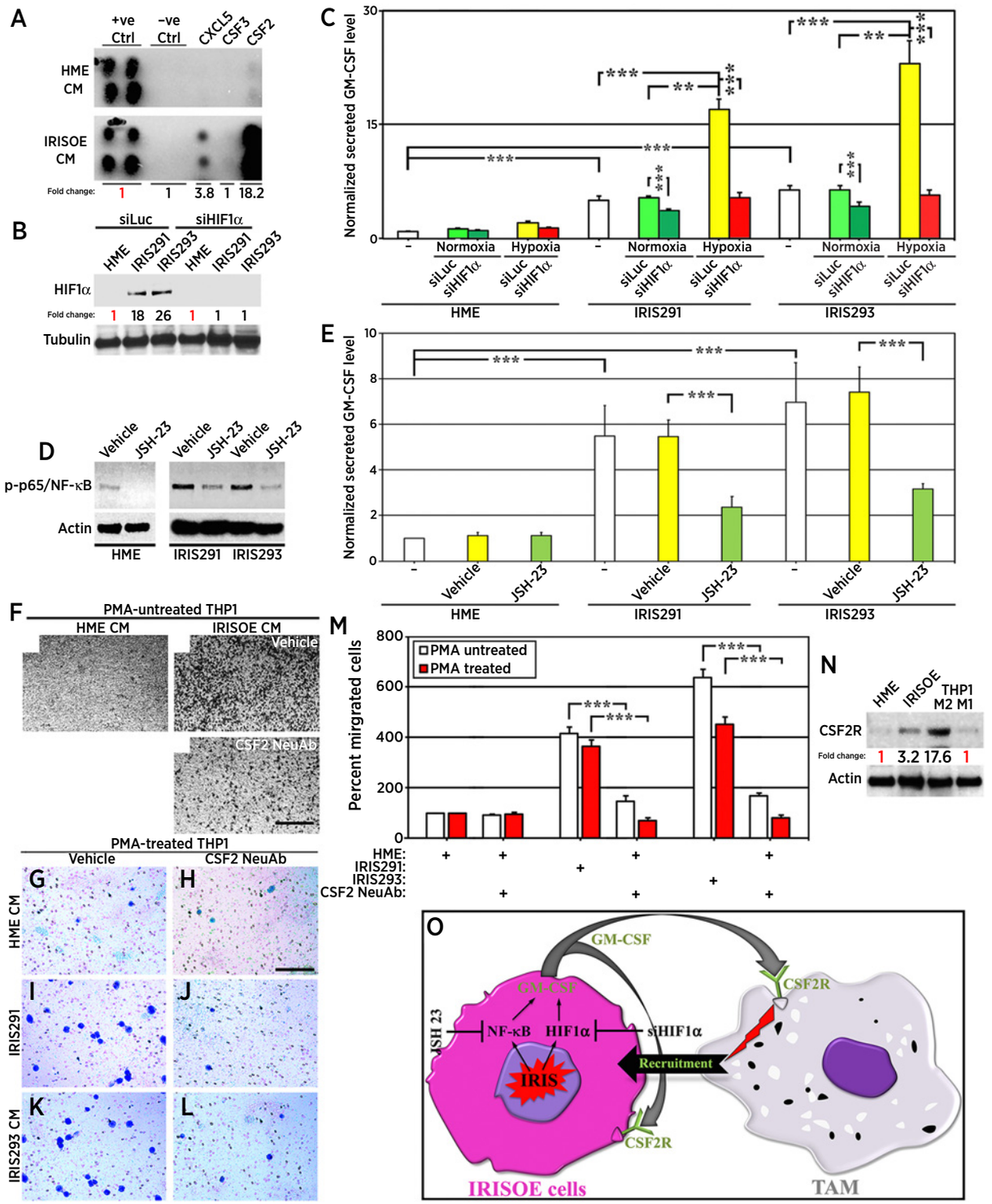

Figure 1.

GM-CSF from IRISOE cells recruits TAMs. **A,** Representative antibody array of indicated CM ($n = 3$/each). **B,** HIF1α expression in indicated cells and conditions. **C,** GM-CSF ELISA in CM of indicated cells conditions ($n = 3$, in triplicates). **D,** Level of p-p65/NF-κB in indicated cells and treatments. **E,** GM-CSF ELISA of indicated cells and treatments ($n = 3$, in triplicates). **F–L,** Migration in Boyden chambers of indicated THP1s toward CM of indicated cells ± GM-CSF NeuAb ($n = 3$, in triplicates). Scale bar, 250 μm (**F**) and 50 μm (**G–L**). **M,** Quantification of data in **F–L**. **N,** Expression of CSF2R in indicated cells. **O,** A schematic representation of the data presented above. **, $P < 0.01$; ***, $P < 0.001$.

Published OnlineFirst January 7, 2020; DOI: 10.1158/0008-5472.CAN-19-2374

cells (**Fig. 1C**). It will be essential to assess the role of HIF2α (30) in this process in the near future.

Inflammation activates NF-κB to promote the expression of cytokines (31). Compared with vehicle-treated HME, IRIS291, and IRIS293 cells, those treated with 10 μmol/L JSH-23 (inhibits NF-κB transcriptional activity; ref. 32) showed significantly lower p-p65/NF-κB level (**Fig. 1D**). This led to significantly decreased GM-CSF secretion from IRIS291 and IRIS293 cells according to ELISA analysis (**Fig. 1E**).

Phorbol 12-myristate-13-acetate (PMA) treatment triggers differentiation of monocytic THP1 cells into none-polarized (M0) macrophages. We layered PMA-untreated or PMA-treated THP1s in 8-μm inserts of Boyden chambers containing HME, IRIS291, or IRIS293 cells CM in the bottom well (media changed daily). Compared with HME CM, IRIS291 or IRIS293 cells CM recruited 400%–600% more PMA-untreated THP1s (72 hours later) that was blocked by GM-CSF neutralizing antibody (NeuAb, **Fig. 1F**). Moreover, HME CM recruited very low number of PMA-treated THP1s (24 hours later) that was not affected by GM-CSF NeuAb (compare **Fig. 1G** with **H**). In contrast, IRIS291 CM recruited significantly higher numbers of PMA-treated THP1 (compare **Fig. 1I** with **G**) that was blocked by GM-CSF NeuAb (compare **Fig. 1J** with **I**), Similarly, IRIS293 CM recruited significantly higher numbers of PMA-treated THP1 (compare **Fig. 1K** with **G**) that was also blocked by GM-CSF NeuAb (compare **Fig. 1L** with **K**). Quantitative analysis of these effects is presented in (**Fig. 1M**). Interestingly, compared with HME cells, IRISOE cells expressed approximately 3-fold higher of the GM-CSF receptor, CSF2Rα (**Fig. 1N**). Compared with M1 polarized THP1s, M2 polarized expressed >15-fold higher of CSF2Rα (**Fig. 1N**).

Taken together, these data suggest that: (i) in the aggressiveness niche, IRISOE stabilizes HIF1α (even under normoxia) (21, 33) and activates NF-κB (17, 22) to trigger GM-CSF expression/secretion from TNBC cells; and (ii) because CSF2Rα is the only high-affinity receptor, GM-CSF recruits M2 more efficiently than M1-polarized macrophages to IRISOE cells (**Fig. 1O**).

GM-CSF triggers TGFβ1 secretion from M2-TAMs

ELISA analysis of CM from siLuc- or siGM-CSF–transfected HME, IRIS291, or IRIS293 cells (48 hours) exposed to normoxia or hypoxia (additional 24 hours) showed that untransfected and untreated THP1s or those exposed to normoxic siLuc- or siCSF2-transfected HME cells CM secrete low levels of TGFβ1 (**Fig. 2A**). Hypoxic siLuc-transfected HME cells CM triggered a 2-fold higher TGFβ1 secretion from THP1s that was blocked by GM-CSF silencing (**Fig. 2A**). In contrast, normoxic siLuc-transfected IRIS291 or IRIS293 cells CM induced approximately 5-fold higher TGFβ1 secretion from THP1s that was increased to >10-fold by the hypoxic CM (**Fig. 2A**). In both situations, GM-CSF silencing blocked the ability of the CM to induce TGFβ1 secretion from THP1s (**Fig. 2A**).

THP1 cells silenced from SMAD5, p65/NF-κB, or ERK (48 hours) were exposed to 50 ng/mL of recombinant GM-CSF for 24 hours, or they were exposed to 50 ng/mL of recombinant GM-CSF in the presence of the vehicle; the STAT5 inhibitor, IQDMA; the NF-κB inhibitor, Bay 11–7082; or the ERK inhibitor, PD98059 (24 hours). ELISA analysis showed recombinant GM-CSF induced >2-fold increase in TGFβ1 secretion by THP1s (vehicle, **Fig. 2B**). Decreasing expression or activity of SMAD5, p65/NF-κB, or ERK (**Fig. 2B**, inset) blockade recombinant GM-CSF–induced TGFβ1 secretion from THP1s (**Fig. 2B**).

IRISOE channels TGFβ1 signaling toward the noncanonical pathway

Compared with HME cells, IRIS291 and IRIS293 express 10- to 20-fold higher of TβRII^{Y424} (constitutively active by autophosphorylation on tumor cells; ref. 34) correlated with a 5- to 10-fold higher cyclin D1 expression (**Fig. 2C**). We transfected the TNBC cell line MDA-MB-468 that overexpresses IRIS (hereafter MDA468; ref. 17) with siLuc or siIRIS (72 hours, **Fig. 2D**). In parallel, we grew HME and IRIS293 cells (24 hours). IRIS-silencing decreased TβRII^{Y424} expression >70%, and cyclin D1 expression >60%, despite increasing p-SMAD2^{S465,S467} level by approximately 3-fold (**Fig. 2D**). Conversely, IRISOE triggered approximately 9-fold increase in TβRII^{Y424} and 5-fold increase in cyclin D1 expression, despite decreasing p-SMAD2^{S465,S467} level by >90% (**Fig. 2D**).

MDA468/shCtrl, MDA468/shIRIS, HME, or IRIS293 cells were all treated with vehicles, 10 ng/mL recombinant EGF, or 5 ng/mL recombinant TGFβ1 (24 hours). Nuclear/chromatin extracts were probed for IRIS and p-SMAD2^{S465,S467} levels. Recombinant EGF treatment did not affect IRIS expression in any of the four cell lines (**Fig. 2E**), while decreased p-SMAD2^{S465,S467} level by approximately 60% in MDA468/shCtrl, and by approximately 70% in IRIS293 cells (**Fig. 2E**). Similarly, recombinant TGFβ1 treatment had no effect on IRIS expression in any of the four cell lines (**Fig. 2E**), decreased p-SMAD2^{S465,S467} level by approximately 60% in MDA468/shCtrl cells and by approximately 50% in IRIS293 cells, and increased it by 2-fold in MDA468/shIRIS cells and HME cells (**Fig. 2E**). Importantly, IRIS-silencing increased p-SMAD2^{S465,S467} level approximately 4-fold, approximately 8-fold, and approximately 12-fold under vehicle, recombinant EGF, or recombinant TGF-β1 treatments, respectively, in MDA468 cells (**Fig. 2E**), and overexpression decreased it by 50% under vehicle, recombinant EGF, or recombinant TGF-β1 treatment in HME cells (**Fig. 2E**). Identical results were obtained using MDA231 and IRIS291 cells.

In total extracts, compared with vehicle, treatment with 5 ng/mL of recombinant TGFβ1 (48 hours) had no effect on IRIS or AKT$^{T308/S473}$ levels, while induced 10-fold increase in p-SMAD3$^{S423/S425}$ level (**Fig. 2F**, black) in HME cells. Compared with vehicle, treatment with 5 ng/mL of recombinant TGFβ1 (48 hours) had no effect on IRIS level, increased p-AKT$^{T308/S473}$ level by 5-fold, while decreased p-SMAD3$^{S423/S425}$ level by 50% in MDA231 and MDA468 cells (**Fig. 2F**, black). Moreover, compared with HME cells, the effect of recombinant TGFβ1 (48 hours) translates to no effect on IRIS level, approximately 15-fold increase in p-AKT$^{T308/S473}$ level, and approximately 95% decrease in p-SMAD3$^{S423/S425}$ level in MDA231 and MDA468 cells (**Fig. 2F**, red).

IRIS291 and IRIS293 cells starved from serum (48 hours) were exposed to 5 ng/mL of recombinant TGFβ1 plus 10 μmol/L of different inhibitors (**Fig. 2G**). In chromatin fraction, under basal condition, IRIS291 and IRIS293 showed low p-SMAD3^{S423,S425} level, and stimulation with recombinant TGFβ1 increased that by approximately 2-fold in both cell lines (**Fig. 2G**). As expected, SMAD3 inhibitor (SMAD3i) decreased recombinant TGFβ1-induced p-SMAD3^{S423,S425} by >3-fold in both cell lines (from 2- to 0.6-fold, **Fig. 2G**). In contrast, inhibiting TβRI/II signaling using LY2109761 or PI3Ḱ/AKT signaling using LY294002 increased p-SMAD3^{S423,S425} level by >5-fold and >3-fold in both cell lines, respectively (**Fig. 2G**).

TGFβ1/TβRI/II triggers EMT/stemness in IRISOE cells through AKT, not SMAD signaling

We treated MDA468 cells in 2D cultures (24 hours) or in 3D-Matrigel (7 days, media/factor/drugs changed every 3rd day) with

Published OnlineFirst January 7, 2020; DOI: 10.1158/0008-5472.CAN-19-2374

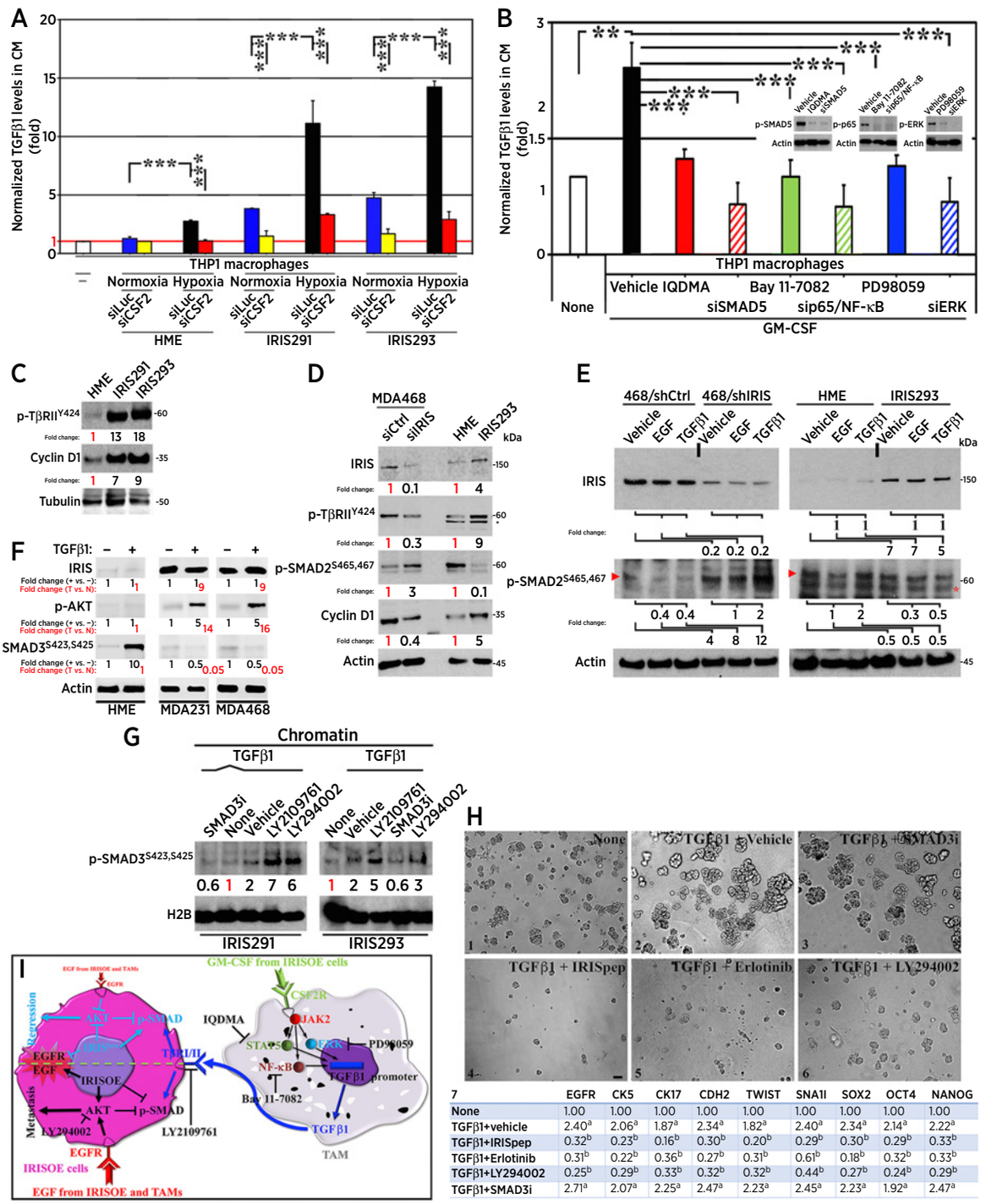

7	EGFR	CK5	CK17	CDH2	TWIST	SNA1I	SOX2	OCT4	NANOG
None	1.00	1.00	1.00	1.00	1.00	1.00	1.00	1.00	1.00
TGFβ1+vehicle	2.40[a]	2.06[a]	1.87[a]	2.34[a]	1.82[a]	2.40[a]	2.34[a]	2.14[a]	2.22[a]
TGFβ1+IRISpep	0.32[b]	0.23[b]	0.16[b]	0.30[b]	0.20[b]	0.29[b]	0.30[b]	0.29[b]	0.33[b]
TGFβ1+Erlotinib	0.31[b]	0.22[b]	0.36[b]	0.27[b]	0.31[b]	0.61[b]	0.18[b]	0.32[b]	0.33[b]
TGFβ1+LY294002	0.25[b]	0.29[b]	0.33[b]	0.32[b]	0.32[b]	0.44[b]	0.27[b]	0.24[b]	0.29[b]
TGFβ1+SMAD3i	2.71[a]	2.07[a]	2.25[a]	2.47[a]	2.23[a]	2.45[a]	2.23[a]	1.92[a]	2.47[a]

Figure 2.

TGFβ1 from macrophages enhances IRISOE cells aggressiveness. **A,** ELISA for TGFβ1 in CM from indicated cells and treatments ($n = 3$, in triplicates). **B,** ELISA for TGFβ1 in CM from indicated cells and treatments ($n = 3$, in triplicates). **C,** Expression of p-TβRII^{Y422} and cyclin D1 in indicated cells ($n = 3$). **D,** Expression of IRIS, p-TβRII^{Y422}, p-SMAD2^{S465,S467}, and cyclin D1 in indicated cells ($n = 3$). **E,** Expression of IRIS and p-SMAD2^{S465,S467} in indicated cells and treatments ($n = 3$). Arrowhead, p-SMAD2^{S465,S467} position; asterisk, nonspecific band. **F,** Expression of IRIS, p-AKT, and p-SMAD3^{S423,S425} in indicated cells and treatments ($n = 3$). **G,** Expression of p-SMAD3^{S423,S425} in indicated cells and treatments ($n = 3$). **H,** Representative images of acini of indicated cells in Matrigel supplemented with indicated factors/drugs ($n = 3$, in triplicates). Scale bar, 50 μm. 7, Normalized mRNA expression (fold) of the indicated factors in indicated cells and treatments. [a], $P = 0.05$; [b], $P = 0.001$ ($n = 3$, in triplicates). **I,** A schematic representation of the data presented above. ***, $P < 0.001$.

Published OnlineFirst January 7, 2020; DOI: 10.1158/0008-5472.CAN-19-2374

none or 5 ng/mL recombinant TGFβ1 plus vehicle, or 2 μmol/L of IRIS inhibitory peptide (hereafter IRISpep; refs. 17, 18, 20–22), 10 μmol/L of erlotinib, LY294002, or SMAD3i (24 hours). In the 3D-Matrigel cultures, recombinant TGFβ1 induced IRIS291 cells to form larger, unorganized, and invasive acini (compare **Fig. 2H**, 1 and 2; ref. 17). Interestingly, while SMAD3i had no effect (**Fig. 2H**, 3), IRISpep (**Fig. 2H**, 4), erlotinib (**Fig. 2H**, 5), and LY294002 (**Fig. 2H**, 6) all blocked these recombinant TGFβ1-induced effects. This was also consistent with the real -time qRT-PCR on total RNAs from the 2D cultures that showed recombinant TGFβ1 increased expression of basal; EGFR, CK5, CD17, and EMT; CDH2, Twist, SnailI, and stemness; and Sox2, Oct4, and Nanog markers (**Fig. 2H**, 7). IRISpep, erlotinib, and LY294002 blocked recombinant TGFβ1-induced expression of these proteins, whereas SMAD3i had no effect (**Fig. 2H**, 7).

Taken together, these data suggest that: (i) GM-CSF secreted from IRISOE cells triggers TGFβ1 production and secretion from TAMs by activating CSF2Rα-induced SMDA5, p65/NF-κB, and/or ERK signaling; and (ii) in combination with (Supplementary Fig. S1B) and our previous studies (16, 17, 18, 20–22), IRISOE-induced EGFR and TβRII expression allows EGF (secreted by IRISOE cells; ref. 28) and TGFβ1 [secreted by TAMs (this study)] to redirect canonical-SMAD signaling that promotes growth suppression, apoptosis, and genomic stability (34) into noncanonical-AKT signaling that promotes aggressiveness in IRISOE cells (**Fig. 2I**).

In vivo evidence for TAM-induced IRISOE tumor aggressiveness

To establish the role of TAMs in promoting IRISOE tumor aggressiveness, *in vivo*, we orthotopically injected 2×10^6 RFP-IRIS291 or RFP-IRIS293 cells alone or admixed with 2×10^5 THP1s ($n = 10$/each, **Fig. 3A**). Compared with alone, THP1 coinjection increased IRIS291 tumor size from 0.9 ± 0.2 cm^3 to 1.8 ± 0.05 cm^3 (2-fold increase), and IRIS293 tumor size from 0.7 ± 0.1 cm^3 to 1.7 ± 0.08 cm^3 (∼3-fold increase) within 10 weeks (**Fig. 3B**). *Ex vivo* analysis showed increased lung (**Fig. 3C**, top arrowheads) and brain (**Fig. 3C**, bottom arrowheads) metastases in mice coinjected with THP1s. THP1 coinjection also led to the death of 7 (IRIS291) and 6 (IRIS293) of the 10 mice (**Fig. 3D**).

To further establish this, 4×10^6 MDA231 cells or MDA468 cells expressing shCtrl or shIRIS (**Fig. 3E**, inset) were injected in female athymic mice (see **Fig. 3E**). Forty days later, tumors and peripheral blood were collected from all mice (**Fig. 3E**). At day 40, shIRIS-expressing tumors were approximately 70% (MDA231, 0.38 ± 0.07 cm^3 vs. 1.2 ± 0.15 cm^3; **Fig. 3F**) and approximately 90% (MDA468, 0.15 ± 0.03 cm^3 vs. 1.3 ± 0.07 cm^3; **Fig. 3G**) smaller than shCtrl-expressing tumors. In addition, only MDA231/shCtrl and MDA468/shCtrl tumors led to the death of 50% of the mice within the 40 days (**Fig. 3G**, left arrows).

Moreover, unpermeabilized single-cell preparations generated from these tumors were colabeled with anti-mouse CD11b (monocytes/macrophage marker) and CSF2R antibodies. We gated forward scatter (as a relative size of the cells) and side scatter (as a measure of the granularity and complexity of the cells) to remove debris and conjugates, and normalized to isotype controls (in all subsequent experiments as well). This analysis revealed that compared with controls, CD11b$^-$ cells increased in MDA231/shIRIS tumors ($73.8\% \pm 3.7\%$ vs. $56.2\% \pm 4.7\%$, $P = 0.0002$) and MDA468/shIRIS tumors ($74.3\% \pm 4.5\%$ vs. $55.6\% \pm 2.7\%$, $P > 0.00005$), while CD11b$^+$ cells decreased in MDA231/shIRIS tumors ($26.2\% \pm 3.7\%$ vs. $43.8\% \pm 4.7\%$, $P = 0.0002$) and MDA468/shIRIS tumors ($25.7\% \pm 4.5\%$ vs. $44.4\% \pm 2.7\%$, $P > 0.00005$; **Fig. 3H**). Importantly, compared with control tumors, CD11b$^-$/CSF2R$^+$ cells increased in MDA231/shIRIS tumors ($13.3\% \pm 1.1\%$ vs. $7.8\% \pm 0.6\%$, $P < 0.000001$) and MDA468/shIRIS tumors ($13.9\% \pm 1.7\%$ vs. $6.9\% \pm 0.6\%$, $P < 0.000001$) and CD11b$^+$/CSF2R$^+$ cells decreased in MDA231/shIRIS tumors ($13.6\% \pm 2.8\%$ vs. $24.1\% \pm 2.4\%$, $P = 0.0002$) and MDA468/shIRIS tumors ($13.2\% \pm 2.9\%$ vs. $23.8\% \pm 2.4\%$, $P > 0.0003$, **Fig. 3H**).

Real-time qRT-PCR analysis performed on total RNA isolated from these tumors showed that compared with MDA231/shCtrl tumors, MDA231/shIRIS tumors contained 8-, 11-, and 5-fold higher HLA-DR, IL12, and iNOS (M1 markers), respectively, while >80% reduced expression of CD206, CCL17, and Arg1 (M2 markers, **Fig. 3I**, yellow). Similarly, compared with MDA468/shCtrl tumors, MDA468/shIRIS tumors contained 6-, 10- and 9-fold higher of HLA-DR, IL-12, and iNOS, respectively, while >90% reduction in CD206, CCL17, and ARG1 levels (**Fig. 3I**, red). Finally, ELISA analysis showed that compared with naïve mice ($n = 40$, **Fig. 3J**, top/white), MDA231/shCtrl or MDA468/shCtrl tumor–bearing mice ($n = 10$/each) showed 12- to 15-fold higher, while MDA231/shIRIS or MDA468/shIRIS tumors–bearing mice ($n = 10$/each) showed only 3- to 5-fold higher circulating GM-CSF and TGFβ1 (>60% decrease, **Fig. 3J**).

Taken together, these data suggest that: (i) the bidirectional interaction with TAMs enhances IRISOE cells' aggressiveness, *in vivo*; and (ii) IRIS silencing decreases TNBC tumors size, circulating GM-CSF, and TGFβ1 levels, and the number of CSF2R$^+$ macrophages recruited into these tumors (**Fig. 3K**).

Syngeneic model for the proposed bidirectional interaction

The BALB/c TNBC tumor cell line, 4T1 (35), overexpress Iris (mouse IRIS homolog; ref. 36) when compared with normal mouse HC11 cell line. We developed two short hairpin RNAs, shIris1 and shIris2 that target Iris intron 11 part and decrease Iris expression in 4T1 cells by >95% (**Fig. 4A**).

We injected 1×10^5 4T1/shCtrl, 4T1/shIris1, or 4T1/shIris2 cells ($n = 8$/each) in female BALB/c mice (**Fig. 4B**). Upper limits were approximately 0.5 cm^3 tumor volume or 40 days. The 4T1/shCtrl cells formed 0.58 ± 0.1 cm^3 tumors by day 20, while 4T1/shIris1 cells 0.13 ± 0.09 cm^3 (>75% reduction, $P < 0.000001$), and 4T1/shIris2 cells 0.07 ± 0.06 cm^3 (>85% reduction, $P < 0.000001$) tumors by day 40 (**Fig. 4C**).

We injected 5×10^5 4T1/shCtrl cells or 4T1/shIris1 cells ($n = 10$/each) in female BALB/c mice (**Fig. 4B**). Upper limits were approximately 1.0 cm^3 tumor volume or 30 days. The 4T1/shCtrl cells formed 1.3 ± 0.1 cm^3 tumors by day 20, while 4T1/shIris1 cells 0.59 ± 0.2 cm^3 tumors (>55% reduction, $P = 0.000002$) by day 30 (**Fig. 4D**). ELISA analysis on sera isolated from these mice showed that compared with naïve mice, 4T1/shCtrl tumor–bearing mice circulation contained 10.1 ± 1.1- and 13.3 ± 0.8-fold higher GM-CSF and TGFβ1, respectively, while 3.3 ± 1.0- and 3.9 ± 0.6-fold, respectively (>60% decrease, **Fig. 4E**) in 4T1/shIris1 tumor–bearing mice.

To evaluate the tumor-infiltrating myeloid compartment within these tumors, unpermeabilized single-cell preparations labeled with anti-mouse FITC-CD11b and PE-F4/80 or PE-CSF2R antibodies were FACS analyzed. The 4T1/shCtrl tumors contained approximately 50% CD11b$^-$ and approximately 50% CD11b$^+$ fractions (**Fig. 4F**), increased to approximately 75% and approximately 25%, respectively, in 4T1/shIris1 tumors (**Fig. 4F**). Compared with 4T1/shCtrl tumors, 4T1/shIris1 tumors showed increase in M1 population (CD11b$^-$/F4/80$^+$ cells, $27.5\% \pm 2.6\%$ vs. $53.7\% \pm 2.9\%$, $P = 0.00004$), and decrease in M2 population (CD11b$^+$/F4/80$^+$ cells, $46.2\% \pm 3.4\%$ vs. $22.9\% \pm 1.9\%$, $P = 0.00009$), and myeloid-derived suppressor cell population (CD11b$^+$/F4/80$^-$ cell; ref. 37; 2.9 ± 0.5 vs. $1.6\% \pm 1.9\%$, $P = 0.00271$; **Fig. 4F** and **G**).

Published OnlineFirst January 7, 2020; DOI: 10.1158/0008-5472.CAN-19-2374

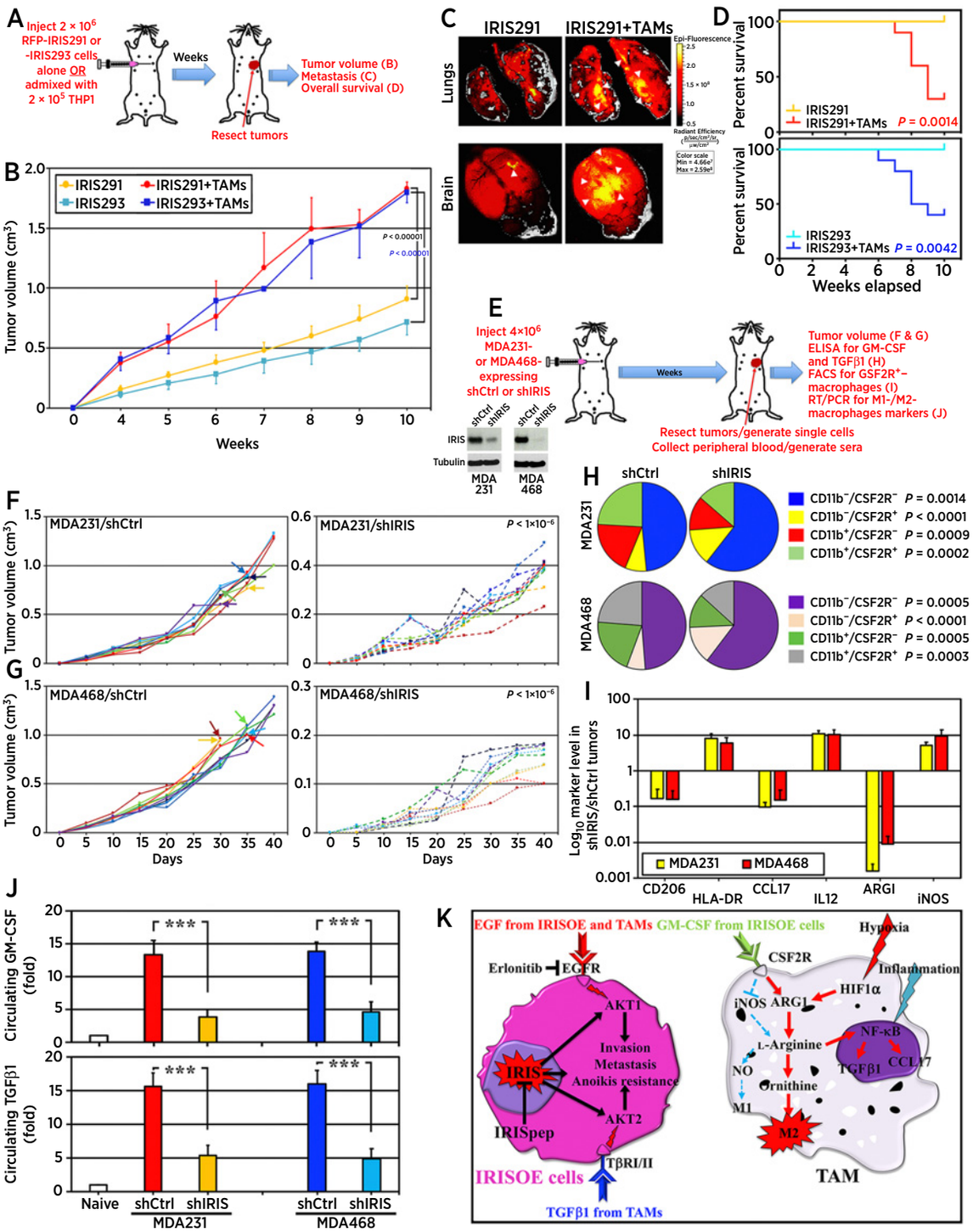

Figure 3.

Bidirectional interaction between IRISOE cells and M2-TAMs. **A,** Schematic description of the assays below. **B,** Volume of tumors in athymic mice injected with 2×10^6 of RFP-IRIS291 or -IRIS293 alone ($n = 10$/each) or admixed with 2×10^5 THP1s ($n = 10$/each). **C,** IRIS291 lung (top) and brains (bottom) metastasis in mice in **A**. Identical results were obtained with IRIS293 cells. **D,** OS in indicated mice injected with indicated cells' combinations. **E,** Schematic description of the assays below (insets show IRIS expression). **F** and **G,** Volume of tumors developed in athymic mice injected with indicated cells (arrows indicate the death of the mice). **H,** Percentage of indicated fractions in indicated tumors. **I,** Log_{10} of indicated markers in $CD11b^+$ cells isolated from indicated tumors. **J,** Level of GM-CSF and TGFβ1 in sera from mice bearing indicated tumors. **K,** Schematic representation of the data presented above. ***, $P < 0.001$.

Published OnlineFirst January 7, 2020; DOI: 10.1158/0008-5472.CAN-19-2374

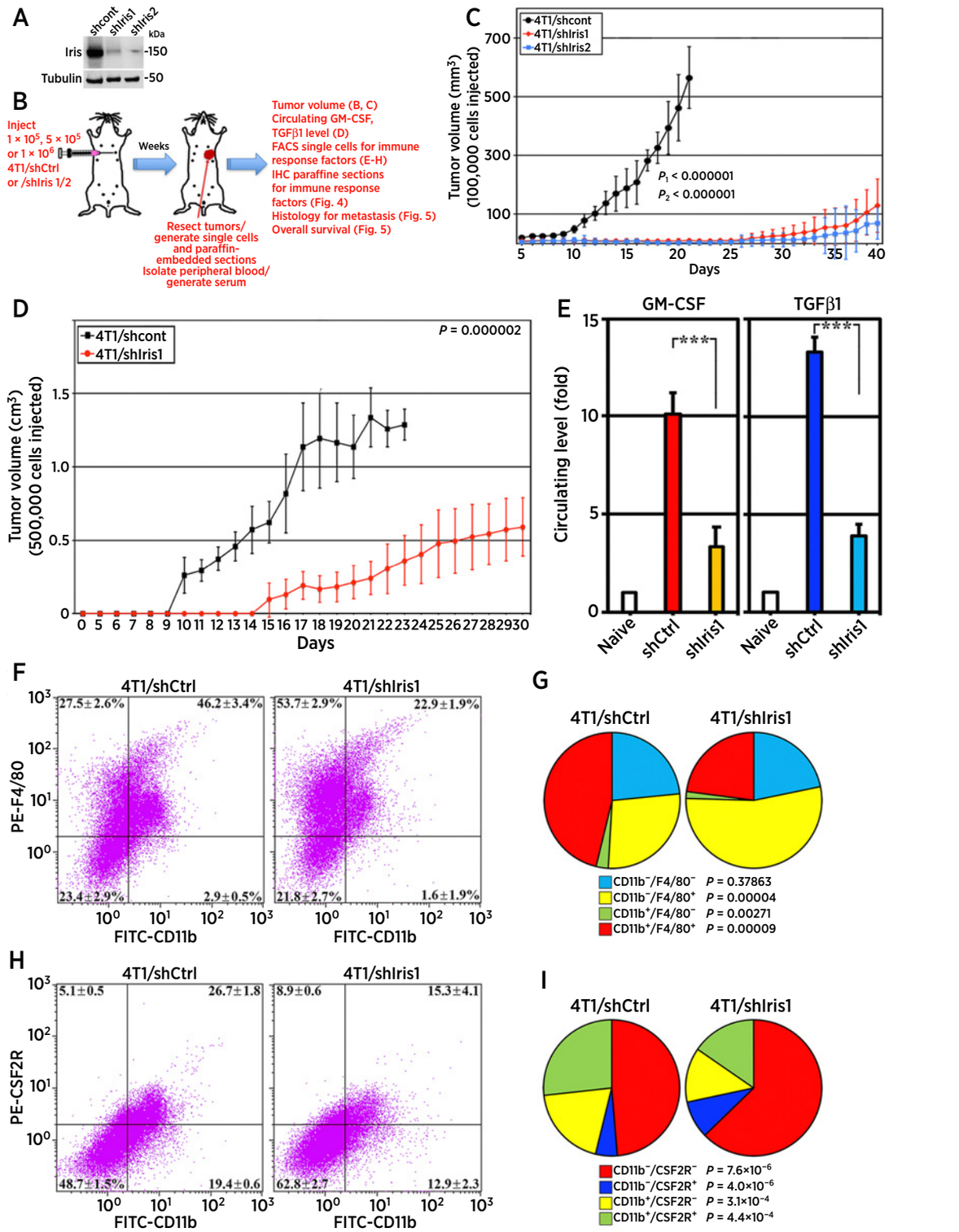

Figure 4.

Syngeneic model for the bidirectional interaction of IrisOE cells and TAMs. **A,** Iris expression in 4T1/shCtrl, 4T1/shIris1, or 4T1/shIris2. **B,** Schematic description of the assays below. **C** and **D,** Volume of tumors developed in BALB/c mice injected with indicated cells. **E,** Levels of GM-CSF and TGFβ1 in the circulation of indicated mice. **F** and **G,** Percentage of indicated cell fractions in indicated tumors. **H** and **I,** Percentage of indicated fractions in indicated tumors. ***, $P < 0.001$.

Published OnlineFirst January 7, 2020; DOI: 10.1158/0008-5472.CAN-19-2374

In addition, compared with 4T1/shCtrl tumors, in 4T1/shIris1 tumors the $CD11b^-/CSF2R^-$ (48.7% ± 1.5% vs. 62.8% ± 2.7%, $P = 7.6 \times 10^{-6}$), and $CD11b^-/CSF2R^+$ (5.1% ± 0.5% vs. 8.9% ± 0.6%, $P = 4.0 \times 10^{-6}$) populations increased (**Fig. 4H** and **I**). In contrast, the $CD11b^+/CSF2R^-$ (19.4% ± 0.6% vs. 12.9% ± 2.3%, $P =$ 0.00031), and $CD11b^+/CSF2R^+$ (26.7% ± 1.8% vs. 15.3% ± 4.1%, $P =$ 0.00044) populations decreased (**Fig. 4H** and **I**).

Indeed, paraffin-embedded sections from these tumors IHC stained for myeloid cells' markers (**Fig. 4B**) confirmed the lack of CSF2R-expressing M2 $CD206^+$-TAMs within 4T1/shIris tumors (compare **Fig. 5A** with **B**). In fact, these analyses also showed that 4T1/shCtrl tumors contained 30.8 ± 7.3 $F4/80^+$ cells/high power field (HPF) and 7.5 ± 3.1 $CD206^+$ cells/HPF, while 4T1/shIris1 tumors contained 18.7 ± 4.9 $F4/80^+$ cells/HPF (>40% decrease, $P < 0.000001$) and 1.1 ± 1.1 $CD206^+$ cells/HPF (>80% decrease, $P <$ 0.000001; **Fig. 5C** and **D**). Moreover, 4T1/shCtrl tumors contained 25.5 ± 5.5 $CD25^+$ cells/HPF and 31.3 ± 4.6 $FOXP3^+$ cells/HPF, while 4T1/shIris1 tumors contained 9.8 ± 3.5 $CD25^+$ cells/HPF (>60% decrease, $P < 0.000001$) and 15.3 ± 2.9 $FOXP3^+$ cells/HPF (>50% decrease, $P < 0.000001$; **Fig. 5E** and **F**). Finally, according to IHC (**Fig. 5G**) and FACS analysis performed on single-cell preparations from these tumors (**Fig. 5H**), 4T1/shCtrl tumors contained 25.7% ± 2.7% $CD8^+$ and showed almost complete absence of PD-1^+ cells, while 4T1/shIris1 tumors contained 38.1 ± 4.2 $CD8^+$ cells (∼50% increase, $P = 0.0001$) and massive number of PD-1^+ cells (**Fig. 5G** and **H**).

Taken together, these data suggest that: (i) like IRIS, depleting Iris also reduces TNBC cells ability to form tumors; and (ii) the bidirectional interaction between IrisOE cells and TAMs through GM-CSF and TGFβ1 triggers immunosuppressive microenvironment within TNBC tumors, including high levels of CSF2R-expressing M2 $F4/80^+/CD206^+$ TAMs and $CD25^+/FOXP3^+$ regulatory T cells, while lower levels of $CD8^+$/PD-1^+ cytotoxic T cells (CTL, **Fig. 5I**).

IRISOE/IrisOE triggers tumor metastasis

We injected 1×10^6 of 4T1/shCtrl or 4T1/shIris2 cells ($n = 10$/cells) in female BALB/c mice (**Fig. 4B**). The limit was death from the disease within 40 days. Tumors, adrenal glands, brains, hearts, kidneys, livers, lungs, and spleens were collected from each anesthetized mouse, paraffin-embedded on a single block, sectioned at 4 μm, and hematoxylin and eosin–stained (**Fig. 4B**). As expected, 4T1/shCtrl tumors were larger. They showed evidence of aggressive TNBC cell morphology, including poorly differentiated epithelial cells with large hyperchromatic nuclei and relatively small cytoplasm (**Fig. 6A**, arrowheads), mesenchymal cells (**Fig. 6A**, arrows), and a large number of mitotic cells (**Fig. 6A**, asterisks). These mice showed relatively low area of internal necrosis throughout the tumor (**Fig 6B**, two-heads arrows). In contrast, 4T1/shIris2 tumors were small in size, contained differentiated epithelial cells only (**Fig. 6C**, arrowheads), and lacked almost completely mitotic cells (**Fig. 6C**). Moreover, compared with 4T1/shCtrl tumors, 4T1/shIris tumors exhibited extensive necrosis throughout the tumor (**Fig 6B** and **D**, two-heads arrows) accompanied by an increase in leukocytes infiltration (**Fig. 6D**, arrows).

In addition, compared with lungs from 4T1/shCtrl cell–injected mice, the lung of 4T1/shIris cell–injected mice were free from metastasis (compare **Fig. 6E** and **F** with **G** and **H**). Similarly, compared with livers from 4T1/shCtrl cell–injected mice, the livers of 4T1/shIris cell–injected mice were free from metastasis (compare **Fig. 6I** and **J** with **K** and **L**). Finally, compared with kidneys from 4T1/shCtrl cell–injected mice, the kidneys of 4T1/shIris cell–injected mice were free from metastasis (compare **Fig. 6M** and **N** with **O** and **P**). Interestingly, in the lungs (**Fig. 6F**) and kidneys (**Fig. 6M**), metastasis was found within or close to afferent vessels and in most cases, appeared infiltrative, whereas in the liver were more localized, often appearing spherical (**Fig. 6I** and **J**). More importantly, all mice injected with the 1×10^6 4T1/shCtrl cells ($n = 10$) died within 25 days (**Fig. 6Q**), while only 3 ($n = 10$) mice injected with 1×10^6 4T1/shIris2 cells died by day 40 (**Fig. 6Q**, $P = 0.0001$).

Taken together, these data suggest that IRISOE/IrisOE generates immunosuppressive microenvironment within TNBC tumors that is favorable for the generation of deadly metastatic precursors.

IRIS inactivation triggers immune surveillance within TNBC tumors

We injected 4×10^6 IRIS291 ($n = 20$) and IRIS293 ($n = 20$) cells in female athymic mice (**Fig. 3A**). By day 20, all mice developed approximately 0.5 cm^3 tumors (**Fig. 7A**). Each group was randomized and intratumorally injected with scrambled peptide (**Fig. 7A**, black arrows, $n = 10$/cell line) or the inhibitory IRIS peptide (IRISpep; refs. 17, 22; **Fig. 7A**, red arrows, $n = 10$/cell line) every 3rd day, a total of four times. By day 30, scrambled-injected IRIS291 2° orthotopic mammary tumors were 1.46 ± 0.11 cm^3, and IRIS293 tumors were 1.49 ± 0.11 cm^3, while IRISpep-injected IRIS291 tumors were 0.31 ± 0.08 cm^3 (>75% regression, $P = 0.0002$) and IRIS293 tumors were 0.34 ± 0.14 cm^3 (>75% regression, $P = 0.004$; **Fig. 7A**).

Unpermeabilized single-cell preparations from each tumor were labeled with FITC anti-CD11b and PE anti-CSF2R antibodies. FACS analysis showed scrambled-injected IRIS291 tumors contained 49.7% ± 5.1%, and IRIS293 tumors 47.4% ± 2.1% of $CD11b^-/CSF2R^-$ cells (**Fig. 7B**), while IRISpep-injected IRIS291 tumors 57.1% ± 5.4% (∼20% increased, $P = 0.05$), and IRIS293 tumors 60.2% ± 2.1% (>25% increase, $P < 0.0001$, **Fig. 7B**). Correspondingly, scrambled-injected IRIS291 tumors contained 22.5% ± 2.2%, and IRIS293 tumors 23.7% ± 1.8% of $CD11b^+/CSF2R^+$ cells (**Fig. 7B**), while IRISpep-injected IRIS291 tumors 13.8% ± 3.2% (40% decrease, $P = 0.0009$), and IRIS293 tumors 12.7% ± 1.2% (50% decreased, $P < 0.0001$, **Fig. 7B**).

In addition, ELISA analysis on sera isolated from these mice showed that compared with naïve mice, inactivating IRIS reduced the increase in circulating levels of GM-CSF by 74% and TGFβ1 by 65% in IRIS291 tumor–bearing mice, and by 70% and 65%, respectively, in IRIS293 tumor–bearing mice (**Fig. 7C**).

FACS analysis showed parental HME cell line contained approximately 50% stem-like/$CD44^+CD24^-$ cells, while IRISOE 1° tumors >95% (**Fig. 7D**; ref. 18), the majority of which are also $CD47^+$ (**Fig. 7E**). Within this population in scrambled-injected 2° IRIS293 tumors 3.8% ± 2.5% were $CD44^-/CD47^-$ cells, and 94.7% ± 2.0% $CD44^+/CD47^+$ cells, while in IRISpep-injected tumors 58.1% ± 5.8% were $CD44^-/CD47^-$ cells (>15-fold increase, $P = 0.00011$), and 40.0% ± 5.2% $CD44^+/CD47^+$ cells (∼60% decrease, $P =$ 0.00007, **Fig. 7F** and **G**). Similarly, in scrambled-injected 2° IRIS291 tumors 2.2% ± 0.5% were $CD44^-/CD47^-$ cells, and 96.6% ± 1.4% $CD44^+/CD47^+$ cells (**Fig. 7G**), while in IRISpep-injected tumors 56.8% ± 7.1% were $CD44^-/CD47^-$ cells (>25-fold increase, $P =$ 0.00018), and 42.6% ± 6.9% were $CD44^+/CD47^+$ cells (>55% decrease, $P = 0.00018$, **Fig. 7G**).

Finally, these stem-like/$CD44^+CD24^-$ cells isolated from the 2° IRIS291 and IRIS293 tumors and 1° IRIS292 tumors expressed 80%–90% lower calreticulin and 9- to 10-fold higher PD-L1 on their surface compared with stem-like/$CD44^+CD24^-$ isolated from HME cell line (**Fig. 7H**).

Taken together, these data suggest that: (i) IRISOE increases CD47 (don't-eat-me initiator); (ii) decreases calreticulin (eat-me initiator);

Published OnlineFirst January 7, 2020; DOI: 10.1158/0008-5472.CAN-19-2374

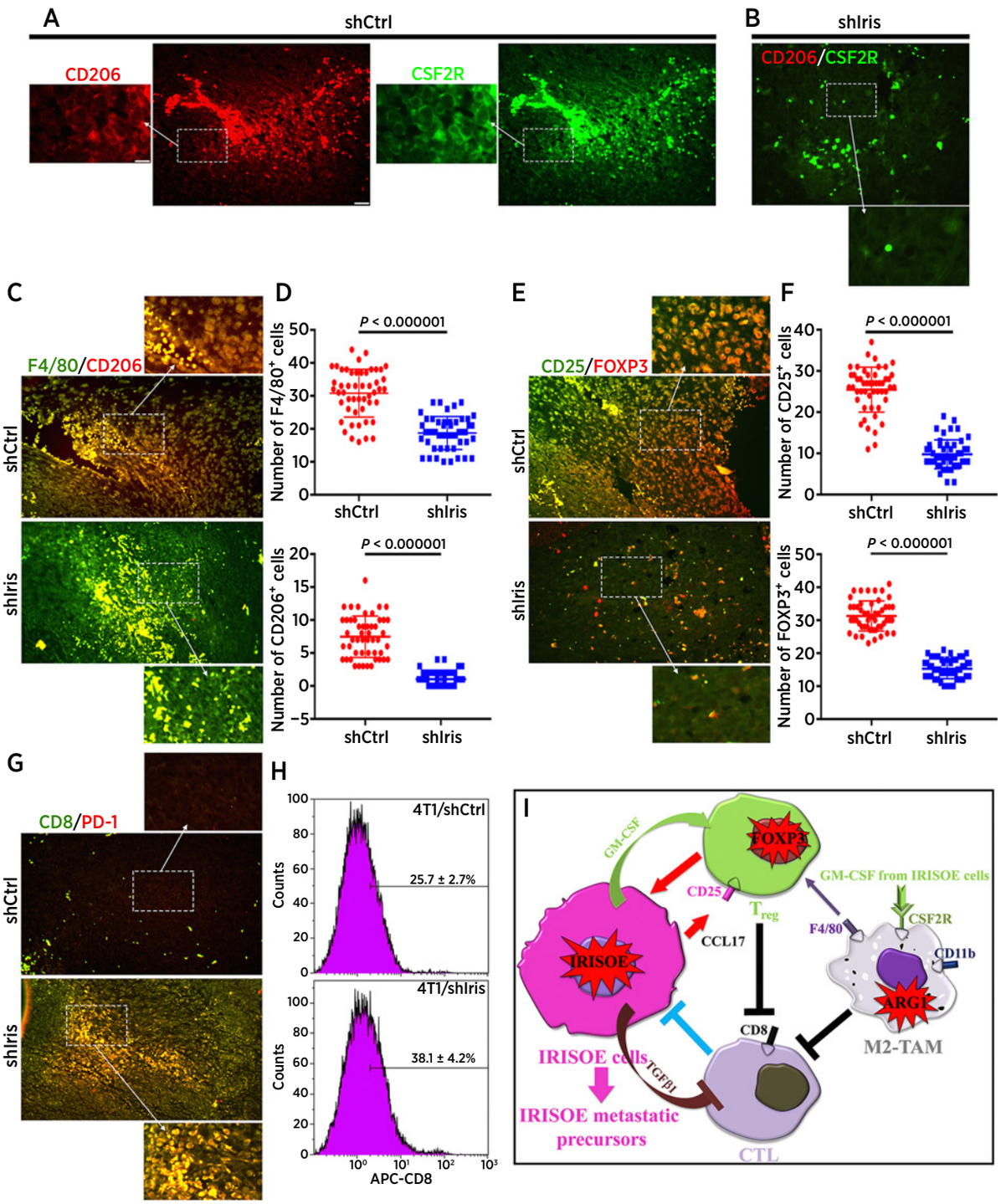

Figure 5.

Immunosuppressive microenvironment in IrisOE TNBC syngeneic tumors. **A** and **B,** Coexpression of M2 biomarker, CD206, and CSF2R in indicated tumors. **C,** Coexpression of CD206 and general macrophage marker F4/80 in indicated tumors. **D,** Quantitative analysis of data in **C**. **E,** Coexpression of the Treg markers CD25 (membranous) and FOXP3 (nuclear) in indicated tumors. **F,** Quantitative analysis of data in **E**. **G,** Coexpression of the CTL markers, CD8 and PD-1 in indicated tumors. **H,** FACS analysis of $CD8^+$ cells in indicated tumors. **I,** Schematic representation of the data presented above. Scale bar, 100 and insets, 25 μm.

Published OnlineFirst January 7, 2020; DOI: 10.1158/0008-5472.CAN-19-2374

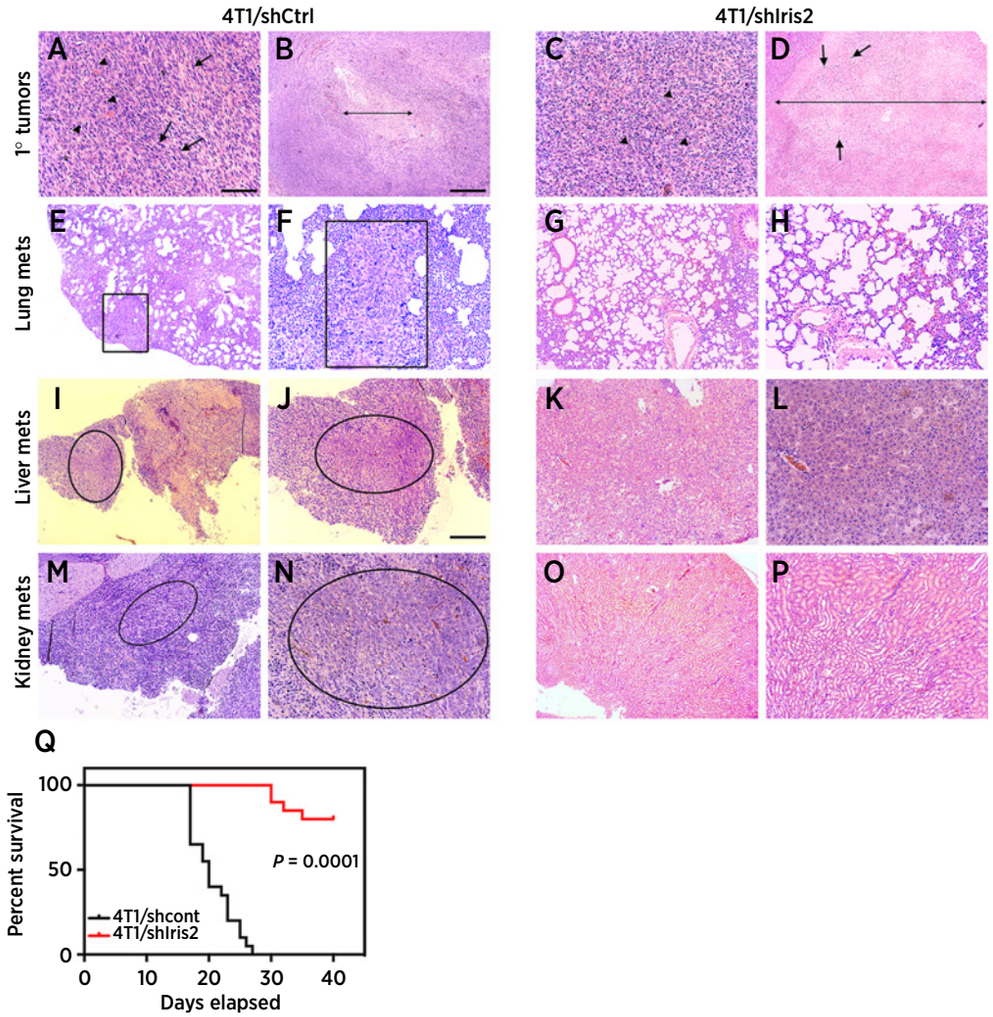

Figure 6.

Iris silencing prevents TNBCs metastasis and enhances mice OS. **A–D,** Representative images of indicated tumors, showing morphologically normal (arrowheads), mesenchymal-like cells (arrows), mitotic cells (asterisks), necrosis (double-headed arrows), and infiltrated lymphocytes (arrows; **D**). Lung metastasis (**E–H**), liver metastasis (**I–L**), and kidney metastasis (**M–P**) in mice injected with indicated cells. Scale bar, 100 μm (**A**, **C**, **F**, **H**, **L**, and **N**), 250 μm (**J**, **K,** and **M**), and 500 μm (**B**, **D**, **E**, **G**, **I**, **O**, and **P**). **Q,** OS in mice injected with 4T1/shCtrl cells (black) or 4T1/shIris2 cells (red).

and (iii) increases PD-L1 expression on TNBC tumor cells, which promotes immunosuppression and TNBC deadly metastasis.

Discussion

Tumor microenvironment plays a crucial role in promoting cancer metastasis. In this study, we showed that within the aggressiveness niche (19) in TNBC tumors, IRISOE cells secrete high levels of GM-CSF. At a low level, GM-CSF exerts an antitumor function by marking cancer cells for elimination by the immune system, or monocyte/macrophage phagocytosis (38). In contrast, high levels of GM-CSF expression exert a protumor function, for example, by enhancing MMPs expression (38). An increased level of GM-CSF in serum indicates poor prognosis in many cancers. In breast cancer, GM-CSF has a crucial role in the establishment of the premetastatic niche in the lungs (7, 39). Increased serum GM-CSF levels in breast cancer–bearing mice promote differentiation of bone marrow–derived cells into neutrophils (tumor-associated neutrophils, TAN) that accumulate in the lungs to promote the metastatic niche (39). Interestingly, our syngeneic model showed that an increase in lung metastasis correlated with high levels of circulating GM-CSF. It remains to be established whether this is accompanied by an increased in the number of TANs in the lungs of these mice.

GM-CSF silencing in IRISOE completely abolished TGFβ1 secretion by THP1s, suggesting bidirectional interaction with macrophages in the form of GM-CSF/TGFβ1. Like GM-CSF, TGFβ1 inhibition or overexpression results in carcinogenesis (40). TGFβ1 binding to TβRII recruits TβRI and activates it. During canonical signaling, activated TβRI/II phosphorylates SMAD2/3 that binds to SMAD4, translocates into the nucleus, and activates or repressors transcription. TGFβ1/TβRI/II can also signal through noncanonical pathways, including AKT (41). The fact that IRISOE blocked SMAD2/3 phosphorylation by TGFβ1 treatment in TNBC cells suggests that IRISOE blocks TGFβ1 canonical signaling and channels it toward noncanonical AKT

Published OnlineFirst January 7, 2020; DOI: 10.1158/0008-5472.CAN-19-2374

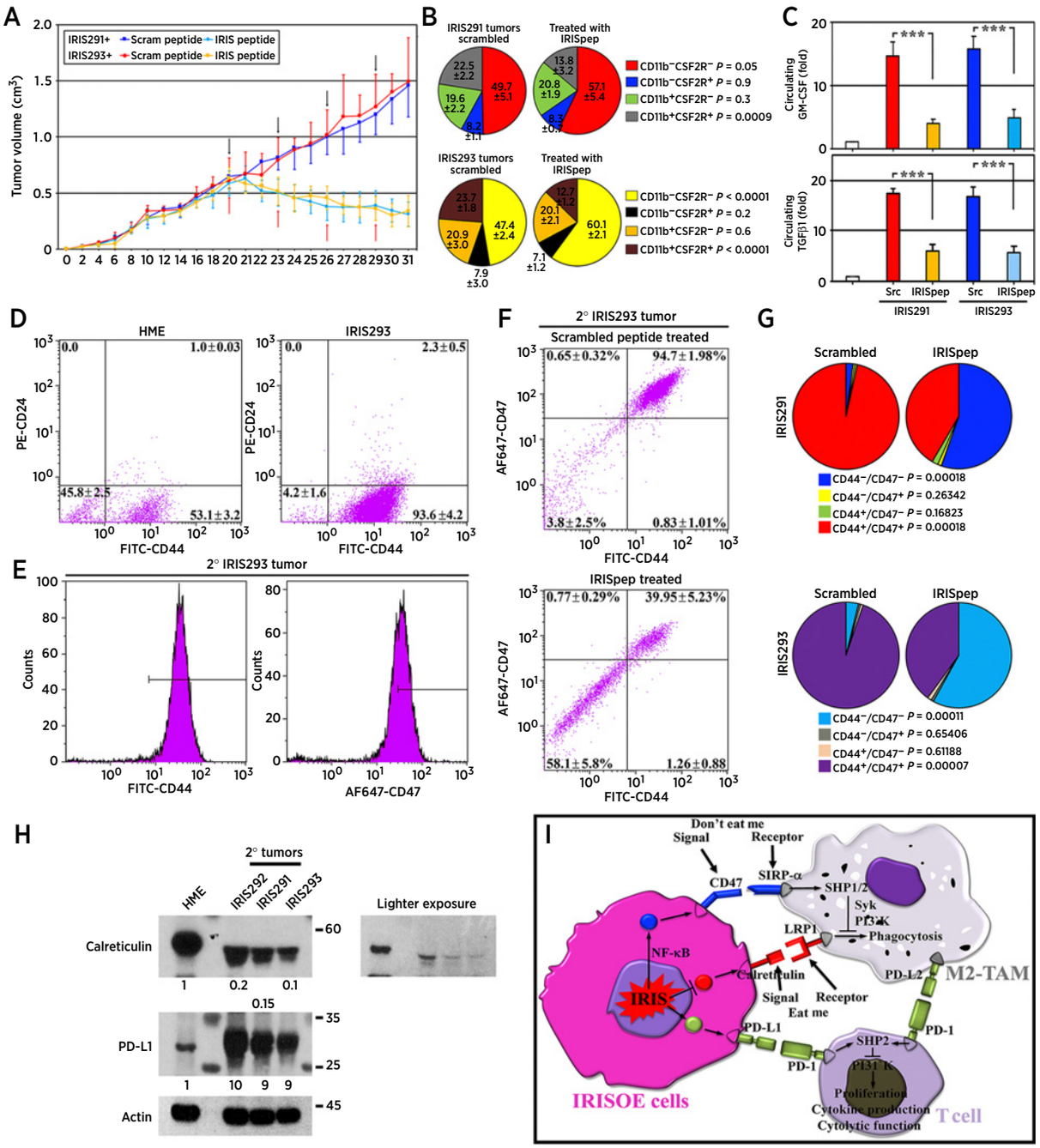

Figure 7.

IRIS inactivation triggers immunity in TNBC tumors. **A,** Volume of established tumors in athymic mice intratumorally injected with scrambled (black arrows) or IRISpep (red arrows). **B,** Percentage of indicated fractions in indicated tumors. **C,** GM-CSF and TGFβ1 ELISA on sera from indicated tumor-bearing mice. **D,** FACS for CD44 and CD24 staining in indicated cells. **E,** FACS for CD44 (left) and CD47 (right) in 2° IRIS293 tumors. The figures are representative of 10 tumors. **F,** FACS for CD44/CD47 on indicated tumors. **G,** Summary of tumors IRIS291 and IRIS293 data shown in **F**. *P* values are shown. **H,** Expression of calreticulin, PD-L1 in HME, 1° IRIS292, or 2° IRIS291 or 2° IRIS293 tumors. The data are representative of five tumors/cell line. **I,** Schematic representation of the data presented above. ***, $P < 0.001$.

signaling, perhaps to enhance stemness/EMT/aggressiveness in TNBC cells. Although we do not yet know the mechanism involved, IRISOE may upregulate one or more of the SMAD2/3 antagonistic pathways (42). We are evaluating this possibility. However, our data present another possible scenario. IRISOE upregulation of an autocrine EGF/EGFR signaling in TNBC cells (17, 22) could block TGFβ1/TβRI/II canonical signaling (43) and enhances noncanonical signaling to increase TNBC cells aggressiveness (**Fig. 2I**).

Published OnlineFirst January 7, 2020; DOI: 10.1158/0008-5472.CAN-19-2374

By inhibiting the "eat-me" signal and activating the "don't eat-me" signal in macrophages, IRISOE effectively renders macrophages within the tumors into nonphagocytic/cytokine-producing factories (**Fig. 7I**). How does IRISOE promote CD47 and suppress calreticulin expression in TNBC cells, remains to be seen? However, HIF1α, NF-κB/p65, and AKT are all known inducers of CD47 and at the same time, are upregulated in IRISOE in TNBC cells (16, 17, 18–22). Calreticulin is an endoplasmic reticulum resident that facilitates the folding of MHC class I molecules. Suppressing its expression would also influence antigen presentation to cytotoxic T cells within the tumor.

A significant obstacle toward an effective TNBC tumor vaccine is the inefficient stimulation of immune cells present within the tumor (44). Reversing this immunosuppression requires activation of CTLs, and suppression of any immune inhibitory elements within the tumor, for example, M2 macrophages (45). In fact, in TNBC tumors, chemotherapies induce the coordinated transcriptional induction of CD47 and PD-L1 mRNAs and proteins expression, leading to T-cell anergy or death (46). Interestingly, we recently showed that chemotherapies upregulate IRIS expression (17, 22). Moreover, during cancer progression, the continuous antigenic stimulation results in T-cell exhaustion (47). PD-1 expression is a common feature of exhausted CD8 T cells, and blockade of PD-1 restores T-cell function *in vivo* (48). Besides, the PD-L1 blockade could lead to a proinflammatory macrophage phenotype, for example, production of higher levels of TNFα and IL12 (49). Our data combined implicate inhibiting IRIS expression or activity (with a specific drug, ongoing) could eliminate the IRISOE/CD47^{+}/PD-L1^{+}/stem-like cell populations within TNBCs involved in the tumors immune evasion, chemo resistance, and metastases. Alternatively, blocking PD-1 or PD-L1 signaling in IRISOE TNBC tumors could rescue exhausted CTLs, and increase the size, proliferation, and survival of macrophages within the tumor by upregulating expression of the MHCII and the costimulatory molecule CD86 (49) and elicit an endogenous and synergistic innate and adaptive immune response against these IRISOE TNBC tumors.

Disclosure of Potential Conflicts of Interest

No potential conflicts of interest were disclosed.

Disclaimer

The funding body had no role in the design of the study and collection, analysis, interpretation of data, and writing the article.

Authors' Contributions

Conception and design: W.M. ElShamy
Development of methodology: B.T. Paul, W.M. ElShamy
Acquisition of data (provided animals, acquired and managed patients, provided facilities, etc.): E. Sami, W.M. ElShamy
Analysis and interpretation of data (e.g., statistical analysis, biostatistics, computational analysis): J.A. Koziol, W.M. ElShamy
Writing, review, and/or revision of the manuscript: J.A. Koziol, W.M. ElShamy
Administrative, technical, or material support (i.e., reporting or organizing data, constructing databases): W.M. ElShamy
Study supervision: W.M. ElShamy
Other (performed experiments): E. Sami, W.M. ElShamy

Acknowledgments

W.M. ElShamy is Dr. Lawrence & Mrs. Bo Hing Chan Tseu, American Cancer Society Research Scholar. This research is supported by an NCI grant R01 CA194447.

The costs of publication of this article were defrayed in part by the payment of page charges. This article must therefore be hereby marked *advertisement* in accordance with 18 U.S.C. Section 1734 solely to indicate this fact.

Received August 3, 2019; revised October 20, 2019; accepted December 31, 2019; published first January 7, 2020.

References

1. Ugel S, De Sanctis F, Mandruzzato S, Bronte V. Tumor-induced myeloid deviation: when myeloid-derived suppressor cells meet tumor-associated macrophages. J Clin Invest 2015;125:3365–76.
2. Murray PJ, Allen JE, Biswas SK, Fisher EA, Gilroy DW, Goerdt S, et al. Macrophage activation and polarization: nomenclature and experimental guidelines. Immunity 2014;41:14–20.
3. Burgess AW, Camakaris J, Metcalf D. Purification and properties of colony-stimulating factor from mouse lung-conditioned medium. J Biol Chem 1977;252:1998–2003.
4. Cook AD, Braine EL, Hamilton JA. Stimulus-dependent requirement for granulocyte-macrophage colony-stimulating factor in inflammation. J Immunol 2004;173:4643–51.
5. Morrissey PJ, Bressler L, Park LS, Alpert A, Gillis S. Granulocyte-macrophage colony-stimulating factor augments the primary antibody response by enhancing the function of antigen-presenting cells. J Immunol 1987;139:1113–9.
6. Su S, Liu Q, Chen J, Chen J, Chen F, He C, et al. A positive feedback loop between mesenchymal-like cancer cells and macrophages is essential to breast cancer metastasis. Cancer Cell 2014;25:605–20.
7. Reggiani F, Bertolini F. GM-CSF promotes a supportive adipose and lung microenvironment in metastatic breast cancer. Oncoscience 2017;4:126–7.
8. Weiskopf K. Cancer immunotherapy targeting the CD47/SIRPalpha axis. Eur J Cancer 2017;76:100–9.
9. Feng M, Chen JY, Weissman-Tsukamoto R, Volkmer JP, Ho PY, McKenna KM, et al. Macrophages eat cancer cells using their own calreticulin as a guide: roles of TLR and Btk. Proc Natl Acad Sci U S A 2015;112:2145–50.
10. Agata Y, Kawasaki A, Nishimura H, Ishida Y, Tsubata T, Yagita H, et al. Expression of the PD-1 antigen on the surface of stimulated mouse T and B lymphocytes. Int Immunol 1996;8:765–72.
11. Day CL, Kaufmann DE, Kiepiela P, Brown JA, Moodley ES, Reddy S, et al. PD-1 expression on HIV-specific T cells is associated with T-cell exhaustion and disease progression. Nature 2006;443:350–4.
12. Yamazaki T, Akiba H, Iwai H, Matsuda H, Aoki M, Tanno Y, et al. Expression of programmed death 1 ligands by murine T cells and APC. J Immunol 2002;169:5538–45.
13. Dong H, Zhu G, Tamada K, Flies DB, van Deursen JM, Chen L. B7-H1 determines accumulation and deletion of intrahepatic CD8(+) T lymphocytes. Immunity 2004;20:327–36.
14. Ghebeh H, Mohammed S, Al-Omair A, Qattan A, Lehe C, Al-Qudaihi G, et al. The B7-H1 (PD-L1) T lymphocyte-inhibitory molecule is expressed in breast cancer patients with infiltrating ductal carcinoma: correlation with important high-risk prognostic factors. Neoplasia 2006;8:190–8.
15. ElShamy WM, Livingston DM. Identification of BRCA1-IRIS, a BRCA1 locus product. Nat Cell Biol 2004;6:954–67.
16. Shimizu Y, Luk H, Horio D, Miron P, Griswold M, Iglehart D, et al. BRCA1-IRIS overexpression promotes formation of aggressive breast cancers. PLoS One 2012;7:e34102.
17. Blanchard Z, Paul BT, Craft B, ElShamy WM. BRCA1-IRIS inactivation overcomes paclitaxel resistance in triple negative breast cancers. Breast Cancer Res 2015;17:5.
18. Sinha A, Paul BT, Sullivan LM, Sims H, El Bastawisy A, Yousef HF, et al. BRCA1-IRIS overexpression promotes and maintains the tumor initiating phenotype: implications for triple negative breast cancer early lesions. Oncotarget 2017;8:10114–35.
19. ElShamy WM, Sinha A, Said N. Aggressiveness niche: can it be the foster ground for cancer metastasis precursors? Stem Cells Int 2016;2016:4829106.
20. Ryan D, Paul BT, Koziol J, ElShamy WM. The pro- and anti-tumor roles of mesenchymal stem cells toward BRCA1-IRIS-overexpressing TNBC cells. Breast Cancer Res 2019;21:53.

Published OnlineFirst January 7, 2020; DOI: 10.1158/0008-5472.CAN-19-2374

21. Ryan D, Sinha A, Bogan D, Davies J, Koziol J, ElShamy WM. A niche that triggers aggressiveness within BRCA1-IRIS overexpressing triple negative tumors is supported by reciprocal interactions with the microenvironment. Oncotarget 2017;8:113294.
22. Paul BT, Blanchard Z, Ridgway M, ElShamy WM. BRCA1-IRIS inactivation sensitizes ovarian tumors to cisplatin. Oncogene 2015;34:3036–52.
23. Livak KJ, Schmittgen TD. Analysis of relative gene expression data using real-time quantitative PCR and the 2(-Delta Delta C(T)) Method. Methods 2001;25:402–8.
24. Ensley JF, Maciorowski Z, Pietraszkiewicz H, Klemic G, KuKuruga M, Sapareto S, et al. Solid tumor preparation for flow cytometry using a standard murine model. Cytometry 1987;8:479–87.
25. Grayson W, Cooper K. Application of immunohistochemistry in the evaluation of neoplastic epithelial lesions of the uterine cervix and endometrium. Curr Diag Path 2003;9:19–25.
26. Hsu SM, Raine L, Fanger H. Use of avidin-biotin-peroxidase complex (ABC) in immunoperoxidase techniques: a comparison between ABC and unlabeled antibody (PAP) procedures. J Histochem Cytochem 1981;29:577–80.
27. Choudhury KR, Yagle KJ, Swanson PE, Krohn KA, Rajendran JG. A robust automated measure of average antibody staining in immunohistochemistry images. J Histochem Cytochem 2010;58:95–107.
28. Bogan D, Meile L, El Bastawisy A, Yousef HF, Zekri AN, Bahnassy AA, et al. The role of BRCA1-IRIS in the development and progression of triple negative breast cancers in Egypt: possible link to disease early lesion. BMC Cancer 2017;17:329.
29. Edge S, Compton C. The American Joint Committee on Cancer: the 7th edition of the AJCC cancer staging manual and the future of TNM. Ann Surg Oncol 2010;17:1471–4.
30. Imtiyaz HZ, Williams EP, Hickey MM, Patel SA, Durham AC, Yuan LJ, et al. Hypoxia-inducible factor 2alpha regulates macrophage function in mouse models of acute and tumor inflammation. J Clin Invest 2010;120:2699–714.
31. Dolcet X, Llobet D, Pallares J, Matias-Guiu X. NF-kB in development and progression of human cancer. Virchows Arch 2005;446:475–82.
32. Ozkok A, Ravichandran K, Wang Q, Ljubanovic D, Edelstein CL. NF-kappaB transcriptional inhibition ameliorates cisplatin-induced acute kidney injury (AKI). Toxicol Lett 2016;240:105–13.
33. Li AG, Murphy EC, Culhane AC, Powell E, Wang H, Bronson RT, et al. BRCA1-IRIS promotes human tumor progression through PTEN blockade and HIF-1alpha activation. Proc Natl Acad Sci U S A 2018;115:E9600–E9.
34. Huang F, Chen YG. Regulation of TGF-beta receptor activity. Cell Biosci 2012;2:9.
35. Guan X, Bryniarski MA, Morris ME. *In vitro* and *in vivo* efficacy of the monocarboxylate transporter 1 inhibitor AR-C155858 in the murine 4T1 breast cancer tumor model. AAPS J 2018;21:3.
36. Pettigrew CA, French JD, Saunus JM, Edwards SL, Sauer AV, Smart CE, et al. Identification and functional analysis of novel BRCA1 transcripts, including mouse Brca1-Iris and human pseudo-BRCA1. Breast Cancer Res Treat 2010;119:239–47.
37. Fang Z, Wen C, Chen X, Yin R, Zhang C, Wang X, et al. Myeloid-derived suppressor cell and macrophage exert distinct angiogenic and immunosuppressive effects in breast cancer. Oncotarget 2017;8:54173–86.
38. Hong IS. Stimulatory versus suppressive effects of GM-CSF on tumor progression in multiple cancer types. Exp Mol Med 2016;48:e242.
39. Quail DF, Olson OC, Bhardwaj P, Walsh LA, Akkari L, Quick ML, et al. Obesity alters the lung myeloid cell landscape to enhance breast cancer metastasis through IL5 and GM-CSF. Nat Cell Biol 2017;19:974–87.
40. Huang JJ, Blobe GC. Dichotomous roles of TGF-beta in human cancer. Biochem Soc Trans 2016;44:1441–54.
41. Mu Y, Gudey SK, Landstrom M. Non-Smad signaling pathways. Cell Tissue Res 2012;347:11–20.
42. Hayashi H, Abdollah S, Qiu Y, Cai J, Xu YY, Grinnell BW, et al. The MAD-related protein Smad7 associates with the TGFbeta receptor and functions as an antagonist of TGFbeta signaling. Cell 1997;89:1165–73.
43. Semlali A, Jacques E, Plante S, Biardel S, Milot J, Laviolette M, et al. TGF-beta suppresses EGF-induced MAPK signaling and proliferation in asthmatic epithelial cells. Am J Respir Cell Mol Biol 2008;38:202–8.
44. Tian H, Shi G, Wang Q, Li Y, Yang Q, Li C, et al. A novel cancer vaccine with the ability to simultaneously produce anti-PD-1 antibody and GM-CSF in cancer cells and enhance Th1-biased antitumor immunity. Signal Transduct Target Ther 2016;1:16025.
45. Barber DL, Wherry EJ, Masopust D, Zhu B, Allison JP, Sharpe AH, et al. Restoring function in exhausted CD8 T cells during chronic viral infection. Nature 2006;439:682–7.
46. Samanta D, Park Y, Ni X, Li H, Zahnow CA, Gabrielson E, et al. Chemotherapy induces enrichment of CD47(+)/CD73(+)/PDL1(+) immune evasive triple-negative breast cancer cells. Proc Natl Acad Sci U S A 2018;115:E1239–E48.
47. Jadhav RR, Im SJ, Hu B, Hashimoto M, Li P, Lin JX, et al. Epigenetic signature of PD-1+ TCF1+ CD8 T cells that act as resource cells during chronic viral infection and respond to PD-1 blockade. Proc Natl Acad Sci U S A 2019;116:14113–8.
48. Pauken KE, Wherry EJ. Overcoming T cell exhaustion in infection and cancer. Trends Immunol 2015;36:265–76.
49. Hartley GP, Chow L, Ammons DT, Wheat WH, Dow SW. Programmed cell death ligand 1 (PD-L1) signaling regulates macrophage proliferation and activation. Cancer Immunol Res 2018;6:1260–73.

Cancer Research
The Journal of Cancer Research (1916–1930) | The American Journal of Cancer (1931–1940)

AACR American Association for Cancer Research

The Immunosuppressive Microenvironment in BRCA1-IRIS–Overexpressing TNBC Tumors Is Induced by Bidirectional Interaction with Tumor-Associated Macrophages

Eman Sami, Bibbin T. Paul, James A. Koziol, et al.

Cancer Res 2020;80:1102-1117. Published OnlineFirst January 7, 2020.